Available online at www.sciencedirect.com
SCIENCE DIRECT
Vision Research 46 (2006) 3336–3359
Vision Research
www.elsevier.com/locate/visres

Multi-area visuotopic map complexes in macaque striate and extra-striate cortex

J.R. Polimeni [a], M. Balasubramanian [b], E.L. Schwartz [a,b,c,*]

[a] Department of Electrical and Computer Engineering, Boston University, Boston, MA 02215, USA
[b] Department of Cognitive and Neural Systems, Boston University, Boston, MA 02215, USA
[c] Department of Anatomy and Neurobiology, Boston University School of Medicine, Boston, MA 02118, USA

Received 8 July 2005; received in revised form 17 February 2006

Abstract

We propose that a simple, closed-form mathematical expression—the *Wedge–Dipole mapping*—provides a concise approximation to the full-field, two-dimensional topographic structure of macaque V1, V2, and V3. A single map function, which we term a map *complex*, acts as a simultaneous descriptor of all three areas. Quantitative estimation of the Wedge–Dipole parameters is provided via 2DG data of central-field V1 topography and a publicly available data set of full-field macaque V1 and V2 topography. Good quantitative agreement is obtained between the data and the model presented here. The increasing importance of fMRI-based brain imaging motivates the development of more sophisticated two-dimensional models of cortical visuotopy, in contrast to the one-dimensional approximations that have been in common use. One reason is that topography has traditionally supplied an important aspect of "ground truth," or validation, for brain imaging, suggesting that further development of high-resolution fMRI will be facilitated by this data analysis. In addition, several important insights into the nature of cortical topography follow from this work. The presence of anisotropy in cortical magnification factor is shown to follow mathematically from the shared boundary conditions at the V1–V2 and V2–V3 borders, and therefore may not causally follow from the existence of columnar systems in these areas, as is widely assumed. An application of the Wedge–Dipole model to localizing aspects of visual processing to specific cortical areas—extending previous work in correlating V1 cortical magnification factor to retinal anatomy or visual psychophysics data—is briefly discussed.

Keywords: Visual cortex; Retinotopic; Quasiconformal mapping; Topographic modeling; Topographic map complex

1. Introduction

The existence of a map of the visual field in cerebral cortex was inferred at the beginning of the twentieth century from human lesion studies (Adams & Horton, 2001; Glickstein & Whitteridge, 1987; Inouye, 1909) and was first observed electrophysiologically in the mid-twentieth century (Daniel & Whitteridge, 1961; Talbot & Marshall, 1941). The first direct observation of this map via brain imaging was made at Brookhaven National Laboratory using an early positron emission tomography (PET) scanner following administration of ^{19}F-labeled 2-deoxyglucose (2DG) to human subjects who viewed a logarithmically structured "ring-ray" stimulus (Schwartz, 1981; Schwartz, Christman, & Wolf, 1984). Subsequent imaging studies using 2DG autoradiography provided much higher detail, indicating that the visuotopic map in macaque primary visual cortex (V1) is well structured down to the level of 100–200 μm (Schwartz, 1994, chap. 9; Tootell, Silverman, Switkes, & DeValois, 1982).

In the 1990s, functional magnetic resonance imaging (fMRI) studies of visual topography provided the primary demonstration, *in vivo*, that fMRI could resolve functional activity within individual brain areas down to the level of several millimeters (e.g., Engel et al., 1994; Ogawa et al., 1992; Sereno et al., 1995). In the near term, the accuracy

* Corresponding author. Fax: +1 617 353 7755.
E-mail address: eric@bu.edu (E.L. Schwartz).

0042-6989/$ - see front matter © 2006 Elsevier Ltd. All rights reserved.
doi:10.1016/j.visres.2006.03.006

of quantitative measurements made through fMRI will improve due to the increasing availability of higher magnetic field strengths [e.g., visual topography data acquired at 7T field strength has been recently demonstrated (Polimeni et al., 2005)] together with advances in fMRI distortion correction techniques. Therefore, understanding of the quantitative details of visual topography must also improve in order to provide a useful *in vivo* validation of these improvements. The modeling work presented in this report is part of a larger, ongoing effort to develop non-invasive, high-resolution brain imaging methodologies and to quantify their accuracy.

The basis for the present investigation into human visual topography is represented by the summary provided in Fig. 1, which was generated from a series of careful lesion studies conducted by Horton and Hoyt (1991a, 1991b). Three key features are immediately evident by visual inspection of the topographic layout of human visual cortex. First, there appears to be a single continuous mapping extending across all three mapped areas—the area boundaries do not disrupt the smoothness of the iso-eccentricity contours. Second, both V2 and V3 appear to be compressed relative to V1 in the direction of the iso-eccentricity contours. Finally, the topographic map reverses at each area border; mathematically, this corresponds to a change in handedness of the underlying coordinate systems in each area (i.e., a ''field sign reversal'').

Although semi-quantitative in nature, the V1–V2–V3 map provided by Horton and Hoyt (1991a) is very well informed and holds up in detail to the quantitative analysis provided below. It also provides a view of the topographic representation over the entire visual field that is currently lacking in fMRI-based observations. The question that it raises, which is addressed in the current report, is how to develop a two-dimensional mathematical model of joint

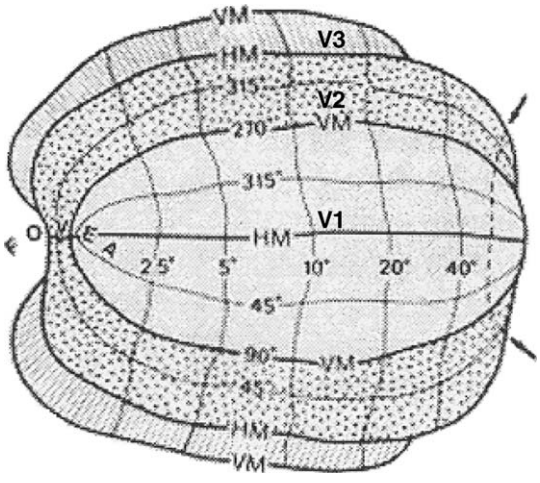

Fig. 1. The topography of human visual areas V1, V2, and V3. The ''HM'' and ''VM'' mark the representations of the horizontal and vertical meridians, respectively. Iso-eccentricity contours run roughly vertically in this layout, and iso-azimuthal contours run roughly horizontally. Reproduced from Horton and Hoyt (1991a).

V1, V2, and V3 topography that is sufficiently well structured so as to provide a basis for current and future quantitative investigations, but that can also supply meaningful characterizations of visual topography.

Here, we have restricted attention to data obtained from the macaque monkey, since the accuracy of these data is considerably higher than that of current human fMRI data, and, crucially, includes valuable topographic data from the peripheral visual field. Encouragingly, several recent fMRI studies have provided quantitative two-dimensional fits to parafoveal human V1 (Duncan & Boynton, 2003) and V1, V2, and V3 (Polimeni et al., 2005) that are in very close agreement to the macaque parameters estimated in this report. This fact is of central importance, since prior estimates of both human and macaque visual topography have been widely scattered (reviewed in Gulyàs, 1997, chap. 16; Levi, Klein, & Aitsebaomo, 1985; Schwartz, 1994; Wilson, Levi, Maffei, Rovamo, & DeValois, 1990, chap. 10). Through the use of well-defined mathematical models and accurate cortical surface flattening, it appears that the variance both within and across the macaque and human species may be far smaller than previously indicated. In this report, we provide a review of several decades of attempts to provide a mathematical description of cortical topography, then present a quantitative application of a recent two-dimensional model to characterize macaque 2DG and electrophysiology data.

In previous work, we showed that a closed-form quasi-conformal mapping of visual field coordinates provides a multi-area, qualitative model of the two-dimensional visuotopic structure of macaque and human cortical areas V1, V2, and V3 (Balasubramanian, Polimeni, & Schwartz, 2002). Conformal mappings provide a good approximation to the structure of macaque V1 visual topography (Schwartz, 1994), but assume local isotropy. Quasiconformal mappings (Ahlfors, 1966b) allow local anisotropy, and thus provide a more general tool for modeling arbitrary two-dimensional, continuous mappings. The proposed mapping is termed the ''Wedge–Dipole'' map, since it is the composition of a constant azimuthal shear ''wedge'' map and a conformal ''dipole'' map that is an extension of the standard log-polar or complex logarithm mapping (Schwartz, 1977b, 1980, 1994).

In the present report, we establish the quantitative validity of the Wedge–Dipole model by fitting the model to two data sets of macaque visual topography data. Statistical analysis supports the quantitative validity of the fits (with correlation coefficient $r \geqslant 0.98$). This result suggests that the V1 and V2 maps share the same conformal parameters, differing only in the handedness of the V2 map [i.e., the V2 topographic map is a mirror reflection of the V1 map around the representation of the vertical meridian (Talbot, 1942)] and in the amount of azimuthal shear: the full-field, global topographic map shows that, on average, V1 is only slightly sheared and V2 is significantly sheared. Based on existing semi-quantitative data, V3 appears as a mirror-reflected version of V2 and we estimate that it is sheared

substantially more than V2 (a precise definition of shear is presented below).

Allman and Kaas (1974a, 1974b) originally suggested that multiple visuotopic areas with shared boundaries can be considered to be a single entity. They applied the term "functional unit" to both V1–V2 and MT–DL in the owl monkey (Allman & Kaas, 1974b, p. 208). Subsequent investigators have used alternative terms: e.g., "functional dyads" (Gattass, Gross, & Sandell, 1981, p. 537), "supra-areal topography" (Rosa, 1997, chap. 4, p. 179), and "map clusters" (Wandell, Brewer, & Dougherty, 2005). In previous work (Balasubramanian et al., 2002), we introduced the term *visuotopic map complex* to describe multiple topographic areas which not only share qualitative features, but which also share a common mathematical underpinning in the form of an explicit visuotopic map function. Thus, beyond providing a quantitative model accounting for the internal topographic details of V1, V2, and V3, the Wedge–Dipole model is capable of jointly modeling V1, V2, and V3 with a single map function, suggesting that these three areas be considered as a single topographic entity, the V1–V2–V3 complex. The quantitative details of the visuotopic map complex in macaque are the subject of the present report.

A preliminary account of this work has appeared in abstract form (Polimeni, Balasubramanian, & Schwartz, 2003).

2. Modeling methods

2.1. Visuotopy and retinotopy: Local and global measurements

2.1.1. Visuotopy

The term *visuotopy* refers to the mapping of points in the visual field to points in cortex, where the mapping is specified by identifying the punctate visual stimulus that maximally excites a spatially localized set of neurons in cortex. The monocular visual field is typically represented as a spherical surface centered at the visual axis and is therefore parameterized using the standard terminology of spherical polar coordinates for *eccentricity*, which for a fixed point in the visual field is typically defined as the angle between the visual axis and the line connecting that point with the anterior nodal point of the eye, and *azimuth*, defined as the projected angle around the visual axis (Morse & Feshbach, 1953). Often, the term "polar angle" is used in place of azimuth in the vision literature.

The idea of a *visuotopic map function* goes back to the early observations of Inouye (1909; see also Adams & Horton, 2001; Glickstein & Whitteridge, 1987), Holmes and Lister (1916), Polyak (1941), and was first electrophysiologically demonstrated by Talbot and Marshall (1941) and Daniel and Whitteridge (1961). During the past fifty years, experimental measurements of visuotopy have been performed using a wide range of techniques, including single-unit and multi-unit microelectrode recording, evoked potentials, 2DG autoradiography, optical recording, PET imaging, and fMRI. The vast majority of this work has been in V1, although, more recently, V2 has received attention, and several studies have been performed in V3 and further extra-striate areas.

2.1.2. Retinotopy

The term *retinotopy*, as a specialization of the category *receptotopy*, refers to the anatomical mapping of the surface of the retina to a central target area such as V1.

The distinction between *retinotopy* and *visuotopy* lies in the non-trivial nature of the mapping of the visual field onto the retina. The visual field is projected onto the retina via an optical system, the eye, but the retina is not precisely spherical, and the wide-angle optics of the eye are not simple. Thus, although the target or range of the topographic mapping is the same (e.g., V1), the domain is different for the case of retinotopy and visuotopy. Furthermore, in studies employing binocular visual stimuli, such as those conducted with fMRI, the mappings of the visual field onto the retinae are generally not in perfect correspondence. Retinal disparity, or differences in how the visual field is projected onto the two retinae, arises when the subject is not fixating at optical infinity and the two eyes are in a state of vergence (Howard & Rogers, 1995). Furthermore, recent studies show that the two eyes will also rotate inward or outward when fixating on targets that are above or below the horizontal plane (Schreiber, Crawford, Fetter, & Tweed, 2001; Van Rijn & Van den Berg, 1993). Virtually all existing measurements to date are visuotopic, with the exception of the recent work of Adams and Horton (2002, 2003b), who measured cortical angioscotomas in the squirrel monkey to produce a high-precision retinotopic map of the "shadows" of retinal blood vessels in V1.

When describing or modeling visuotopic (or retinotopic) maps it is often convenient to assume that the mapping is an invertible one-to-one point-mapping sending zero-dimensional points in the visual (or retinal) coordinate system to zero-dimensional points in the cortical coordinate system. In reality, individual photoreceptor cells may ultimately project to multiple target cortical cells, or individual cortical cells may receive input from multiple photoreceptor cells, in which case a one-to-many or many-to-one mapping would be implemented. This distinction is particularly relevant in machine vision systems that mimic the space variant sampling seen in biological vision systems—in these systems, the sampling and pooling of pixels from the sensory surface is explicit and simplifying assumptions of continuity must be discarded (see, e.g., Rojer & Schwartz, 1990).

2.1.3. Experimental difficulties with visuotopic and retinotopic measurements

One experimental problem associated with visuotopic measurements is that the optical system of the eye is usually not carefully considered. For example, wide-angle eye models (e.g., Drasdo & Fowler, 1974) suggest that there is significant anisotropy, or shear, in the peripheral field due to the optics of the eye. Second, it is difficult to precisely fix the visual axis: paralyzed preparations tend to have an error in the range of 0.5° in the location of the (slowly drifting) fovea (Van Essen, Newsome, & Maunsell, 1984). This can provide a large source of error in a topographic map estimate, since the central 1° of visual field occupies a significant fraction of the entire surface area of V1. Current PET and fMRI experiments depend on human subjects holding exact binocular fixation for tens of minutes—a difficult task to perform reliably. Finally, most current analysis of topographic structure is based on flat approximations of the cortex which are produced either by physical or numerical flattening. The geometrical error, even in optimal numerical flattening, is on the order of 10–20% (Schwartz, Shaw, & Wolfson, 1989b), while the errors in physical flattening can be much larger. In one study, the opercular surface alone of macaque V1, when flattened under glass, showed local error distortions that were as large as 30% (Schwartz, Munsiff, & Albright, 1989a), with considerably larger errors expected for the full macaque V1. For this reason, in the present study we consider only numerically flattened data (see Section 3).

2.1.4. Global measurement: 2DG, cytochrome oxidase, PET, and fMRI

Global measurements of topographic mappings have been performed via metabolic labeling techniques, such as 2DG autoradiography (Schwartz et al., 1989a; Tootell et al., 1982), cytochrome oxidase histochemistry of angioscotomas (Adams & Horton, 2003b), and in human, using 2DG PET scanning (Fox, Miezin, Allman, Van Essen, & Raichle, 1987; Schwartz, 1981; Schwartz et al., 1984), and fMRI (Engel, Glover, & Wandell, 1997; Sereno et al., 1995). Mathematical modeling of the global structure of V1 began with the use of the complex logarithmic mapping (Schwartz, 1977b, 1980), which is agreed to

be a "good approximation" to the central 20° of macaque visual cortex (Dow, Vautin, & Bauer, 1985; Tootell, Silverman, Switkes, & DeValois, 1985; Van Essen et al., 1984), and which is the only closed-form, two-dimensional model currently used for V1 topography that is in general agreement with existing data.

2.1.5. Local measurement: Magnification factor

Despite the fact that quantitative measurement of cortical topography provides one of the clearest applications of computational neuroscience, and one which requires a two-dimensional mathematical analysis, visual topography has been most often summarized in terms of a single one-dimensional magnification function.

Cortical magnification factor was originally defined, in the context of visual topography, as the ratio of the difference in cortical position (in millimeters) to visual field position (in degrees) of a small movement of a visual stimulus (Daniel & Whitteridge, 1961). This quantity is clearly a differential measurement: it is the ratio of small displacements in the range of the topographic map function to small displacements in its domain (retina or visual field). However, it is important to emphasize that the common practice of inferring global characteristics based on a scalar magnification factor is not sufficient—even for the case of a conformal mapping—for the following reasons.

2.1.5.1. The differential of a general two-dimensional map is a matrix, not a scalar. The differential of a general two-dimensional map requires four parameters to be measured at each point, not a single scalar such as magnification factor (Schwartz, 1984). A mapping from a two-dimensional surface (e.g., the visual field or the retina) to a two-dimensional cortical surface can be written as f: $(x,y) \mapsto (u,v)$, where (x,y) represents a point in the domain (e.g., the visual field) and (u,v) represents a point in the range (i.e., the cortex). The differential of the mapping, df, can be represented by the matrix of partial derivatives u_x, u_y, v_x, and v_y. These four parameters are, in the case of visuotopic mapping, the ratio of two orthogonal small steps in the visual field and the corresponding two small, linearly independent steps in the cortex, which are the four partial derivatives that make up the Jacobian matrix (see Schwartz, 1994, for detailed discussion). If a map is conformal and thus locally isotropic, then magnification factor characterizes the map function. For conformal maps, magnification factor is equal to the square root of the determinant of the Jacobian matrix. However, global isotropy does not necessarily follow from local isotropy.

2.1.5.2. A conformal map is (almost) never globally isotropic. It has sometimes been incorrectly assumed in the vision literature that a conformal map, which is *locally* isotropic by definition, is also *globally* isotropic, i.e., that magnification factor is identical along the horizontal, vertical, and all other meridians (e.g., see Tootell et al., 1982, or Sakitt, 1982; cf. Letelier & Varela, 1984; Schwartz, 1985). For the simple conformal map function $k \log(z+a)$, where $z = x + \mathrm{i}y$ is complex valued, the derivative or magnification factor evaluated along the horizontal meridian is $k/(x+a)$, while the magnification factor along the vertical meridian is $k/\sqrt{y^2+a^2}$. This yields a maximum difference of $\sqrt{2}$, i.e., about 40%, at the point where $x = y = a$. This demonstrates that the length of the vertical and horizontal meridians need not be equal, even for manifestly conformal maps such as $k \log(z+a)$. In general, magnification factor is significantly different along different meridians, even when a map is conformal and thus locally isotropic. In the special case where the conformal map is simply a geometric similarity (i.e., a scaling or rigid transformation), then the map is both locally and globally isotropic.

In the light of this fact, it is possible to correct a confusion which can be traced back to one of the earliest studies of cortical magnification. Daniel and Whitteridge (1961) state that linear cortical magnification factor is both locally isotropic and independent of azimuth and therefore identical along the horizontal meridian and vertical meridian representations, which means that the map is both locally and globally isotropic. As discussed above, this is a mathematical impossibility unless the map function were a simple uniform scaling, which follows from the uniqueness property of conformal mappings guaranteed by the Riemann Mapping Theorem (Ahlfors, 1966a). Therefore, the joint requirement of local and global isotropy cannot, in general, be satisfied.

2.2. Canonical two-dimensional topographic mapping

The existence of *continuous* topographic maps is sometimes called into question due to the lack of continuity posed by the existence of multiple feature maps representing other variables across a cortical surface. Ocular dominance columns in V1 (Hubel, Wiesel, & LeVay, 1974; LeVay, Hubel, & Wiesel, 1975) and the columnar systems of V2 (Roe & Ts'o, 1995; Tootell & Hamilton, 1989) are examples which seem to contradict the existence of a single continuous map of visual coordinates to the cortical surface. Therefore, it is important to emphasize the utility of the concept of a topographic map that operates on a scale that is larger than that of individual V1 or V2 columnar systems. We use the term *canonical two-dimensional topographic map* to refer to an empirically defined, scale-dependent summary of these types of data sets. [A similar point of view is adopted by Shipp and Zeki (2002) in the context of V2 visuotopy.] Experimental techniques addressing topography usually do not spatially resolve columnar-level data. The intention of the concept of canonical topography is to explain and summarize experimental data collected mainly via multi-unit recording, 2DG autoradiography, optical recording, cytochrome oxidase staining, or fMRI. In these contexts, there is a *canonical* continuous, two-dimensional map structure. The goal of this report is to provide a mathematical framework within which these levels of supraneuronal architecture can be concisely summarized and conceptualized. The much more difficult problem of jointly characterizing columnar-level and canonical-level topographic data using the mapping formalism (see Landau & Schwartz, 1992, 1994) is outside the scope of the present report.

In two dimensions, a generalization of the class of conformal mappings is the *quasiconformal mappings*, which can be expressed as a composition of a conformal and non-conformal mapping. Conformal mappings are mappings that locally preserve angles and are therefore locally isotropic. Quasiconformal mappings are a natural generalization of conformal mappings that allow for bounded local anisotropy. Thus, quasiconformal mappings represent the most general class of *regular* (non-singular) mappings in two dimensions (Ahlfors, 1966b). Ahlfors and Bers (1960) proved that an arbitrary quasiconformal mapping may be represented as a conformal mapping with respect to a suitable change in metric.

2.3. The monopole mapping

The reciprocal of the V1 magnification factor has been reported to be approximately linear (Schwartz, 1977b; Wilson et al., 1990). The complex logarithm, $w = \log(z)$, with z restricted to the half-disc, is therefore an obvious candidate to model the two-dimensional structure of the mapping, as the magnitude of its derivative is also inverse-linear. However, the complex logarithm has a singularity at the point $z = 0$. One can remove the singular point from the mapping domain by choosing the function $w = k \log(z+a)$, which places the singularity at $z = -a$ (see Figs. 2A and B), where the real parameter k normalizes the area, and the parameter a determines a relative scaling of the size of the foveal representation in cortex. Note that we are implicitly representing the two hemispheres of cortex, and the corresponding visual hemi-fields, as independent maps (see Mathematical Appendix). Since the complex logarithm describes the electrostatic potential in two dimensions of a single charge located at $z = -a$ (Morse & Feshbach, 1953), we call it an *a-monopole mapping* (henceforth simply the *monopole mapping*). The monopole mapping captures the approximate shape of flattened V1, as well as the internal details of the topography (Schwartz, 1977b, 1980). However, it does not adequately capture the far peripheral data where the inverse magnification factor is markedly super-linear (Schwartz, 1983, 1984; Van Essen et al., 1984), nor does it capture the shape of the flattened cortex in its far peripheral-field representation.

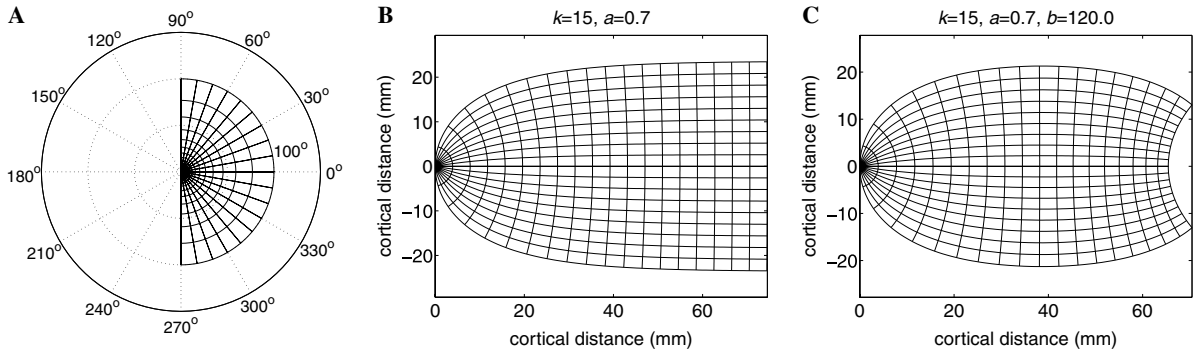

Fig. 2. Iso-azimuth and iso-eccentricity contours mapped through the two complex logarithm models of V1 topography. (A) The right visual hemi-field. Visual field coordinates representing eccentricity and azimuth appear as labeled iso-contours, with the foveal representation at the origin. (B) The *a*-monopole map of the right visual hemi-field. (C) The *ab*-dipole map of the right visual hemi-field. In each diagram, eccentricity increases from left to right. Note that the iso-azimuth contours are located uniformly in visual field coordinates, whereas the iso-eccentricity contours are exponentially located.

Remarkably, the addition of a second logarithmic pole of opposite sign makes up for these deficiencies (Schwartz, 1983), hence the dipole mapping.

2.4. The dipole mapping

In electrostatics, the potential of a pair of opposite unit charges (a dipole) is given by the sum of two oppositely charged monopole potentials: $w = k\ [\log(z+a) - \log(z+b)]$, where the positive charge is at $z = -a$ and the negative at $z = -b$ (Morse & Feshbach, 1953). We shall refer to this function as the *ab-dipole mapping* (henceforth the *dipole mapping*). The second parameter b approximates the shape of the V1 boundary exhibited at the peripheral representation (see Fig. 2C) as well as the super-linearity of the inverse cortical magnification factor in the peripheral field (Schwartz, 1983, 1984; Van Essen et al., 1984), and the real parameter k again normalizes the area. The dipole mapping therefore provides a three-parameter conformal map model of the *full-field* topography of primary visual cortex.[1] The remaining feature to be accounted for is topographic shear.

2.5. Azimuthal shear in V1 and V2

In the next section, we introduce a very simple form of *topographic shear*: a constant compression along the azimuth coordinate direction in each area. (The term "shear" is the technically accepted term to describe local anisotropy, i.e., different "magnification" in different directions, at a given point; see Segel, 1977.) This shear model is consistent with reports (e.g., Roe & Ts'o, 1995, chap. 7, 1997; Rosa, Sousa, & Gattass, 1988; Shipp & Zeki, 2002), that the V2 magnification factor measured in the azimuth direction (perpendicular to the V1–V2 border) is much smaller than that measured in the eccentricity direction (parallel to the V1–V2 border), and that a similarly oriented, although smaller, magnification factor anisotropy exists in V1 (see, e.g., Blasdel & Campbell, 2001). This is an approximation to what has been reported for V1 and V2 along their common boundary, as is evident from casual inspection of numerically flattened maps of the three areas—V2 and V3 appear "squeezed" in the direction perpendicular to their shared boundaries, as shown in Fig. 1.

To quantify the amount of shear observed in a given area, many authors choose to report a *ratio* of one-dimensional magnification factors along different coordinate directions. For example, Van Essen et al. (1984) and Adams and Horton (2003b) report an *anisotropy index* across cortex, which is the ratio of the magnification factor in the eccentricity coordinate direction to the magnification factor in the azimuth coordinate direction. Note that this assumes that the principle axes of the shear are aligned with the coordinate directions of eccentricity and azimuth, as is assumed in our model as well. Thus, we follow the convention of reporting topographic shear by the ratio of magnification factor in the eccentricity direction to magnification factor in the azimuth direction. For example, a 5:2 anisotropy index corresponds to a 2.5 × compression along the azimuth direction relative to the eccentricity direction, resulting in $(\frac{5}{2} - 1) \times 100\% = 150\%$ compressive azimuthal shear.

The magnitude and distribution of V1 shear are somewhat controversial, and at least three distinct statements have been made on this subject over the years. In the following, the particular shear model will be named after the authors of the respective articles.

LeVay et al. shear: LeVay et al. (1975) made electrode penetrations perpendicular to the boundaries of ocular dominance column stripes in layer IV of macaque V1 and found that the local magnification factor was twice as large in the direction parallel to the stripe boundary than in the perpendicular direction (see also Hubel & Wiesel, 1977; Hubel et al., 1974). Since the ocular dominance column stripe boundaries generally intersect the V1–V2 border at right angles, and are therefore aligned with the azimuth coordinate direction there, the findings of LeVay et al. (1975) suggest that the "sub-columnar" topographic representation in layer IV exhibits a anisotropy index of 1:2, eccentricity to azimuth. They suggested that this would allow for an interlacing of the two complete maps for the left and right eye such as to allow for a "supra-columnar" shear of 1:1 in the combined map consisting of the two monocular mappings viewed as a single binocular map. (In this context, *sub-columnar* denotes a scale that is smaller than a single hypercolumn and *supra-columnar* denotes a scale that is larger than a single hypercolumn.)

Tootell, Switkes, Silverman, and Hamilton shear: Based on a macaque 2DG study, Tootell, Switkes, Silverman, and Hamilton (1988) suggested that magnification factor was the same in the two directions (perpendicular and parallel to the local ocular dominance column map) within single ocular dominance column stripes, i.e., a sub-columnar anisotropy index of 1:1, contradicting LeVay et al. (1975). If this were true, the overall, supra-columnar topographic map would need to be grossly

[1] The full dipole model should only be used if there is peripheral-field data available to constrain the value of the b parameter. The value of an unconstrained b parameter can converge to a value close to the value of the foveal parameter, a, when fitting the map to data. In this case, the b parameter, whose purpose is to characterize peripheral-field data, will instead influence the map fit within the central-field. This will lead to both a and b simultaneously characterizing the central-field, producing misleading values for both a and b. Thus, when only central-field data are available the monopole model should be used.

sheared by a factor of about 2:1, eccentricity to azimuth. Thus, the Tootell et al. (1988) shear has no sub-columnar shear, but on average exhibits a large supra-columnar shear.

Blasdel and Campbell shear: Using optical recording in macaque, Blasdel and Campbell (2001) reported a result intermediate to the previous two claims. In this study, the supra-columnar anisotropy was calculated directly by measuring the azimuth and eccentricity magnification factors across 1–4 mm regions of cortex. Magnification factor across multiple pairs of ocular dominance column stripes was averaged together in each calculation, but the measurement was still confined to a small, localized region of V1, resulting in a direct, supra-columnar measurement. Near the vertical meridian, they found a anisotropy index of about 1.5:1; however, much smaller ratios were calculated near the horizontal meridian (1.15:1). They attributed this difference to the lack of order of stripe direction near the horizontal meridian compared to the vertical meridian. Others have also observed that shear is largest near the vertical meridian, while smaller at other locations (Schwartz, 1994; Van Essen et al., 1984), which is in general agreement with the small values of shear reported by Blasdel and Campbell (2001) in regions far from the vertical meridian representation.

The reported shear in V2 (see, e.g., Roe & Ts'o, 1995, 1997; Rosa et al., 1988; Shipp & Zeki, 2002) is less discussed, and there has been to date only one shear model proposed.

Roe and Ts'o shear: Roe and Ts'o (1995) observed that topographic shear in V2 compresses the visual representation in a direction perpendicular to the V2 columnar borders. V2 columns are triply represented in the thick-thin-interstripe columnar system [but see Sincich and Horton (2002) for evidence countering the "triple representation" model]. Roe and Ts'o (1995) found the sub-columnar V2 magnification factor to be highly anisotropic with a ratio of about 2:1 (eccentricity to azimuth), resulting in a supra-columnar shear which Roe and Ts'o (1995) hypothesized to be 6:1, following reasoning similar to that of Tootell et al. (1988) relating sub-columnar shear to supra-columnar topography in V1.

If there were a supra-columnar shear of 2:1 in V1, as suggested by Tootell et al. (1988), it would be unlikely that conformal models of V1 would be as good an approximation as they are (cf. Schwartz, 1994; see also Section 3). All four models of shear share the assumption that the shear axes are aligned with the local columnar system—the ocular dominance system in V1 and the thick-thin-interstripe system in V2. For these reasons, we have adopted a simplifying model in which a uniform azimuthal shear is present in V1 and V2, which we hypothesize to be extended into V3. More complicated, and more plausible, assumptions are possible. The next simplest assumption is that the shear may be modeled as being largely azimuthal but not uniform—it has been observed by Blasdel and Campbell (2001) that the topographic shear is larger near the vertical meridian in V1 and decreases near the representation of the horizontal meridian. This possibility is briefly considered in Section 4 (see Fig. 18).

In the fully general case in which the shear is not constant or aligned with the spherical coordinate directions, it is necessary to compute the magnitude and direction of the shear at each point. This general solution, requiring fitting the Jacobian matrix of the topographic mapping, is described in detail in earlier work (Schwartz, 1984, 1994).

We have found that the simplest assumption, that of constant azimuthal shear, provides a good quantitative fit to the existing data with a minimal number of extra parameters beyond those characterizing the conformal component of the mapping. This will now be demonstrated.

2.6. Model goals

The visual topography of human V1, V2, and V3 is shown diagrammatically in Fig. 1. An inspection of this figure, along with the prior discussion of shear, suggests the following goals for a model of the topography of V1, V2, and V3.

G1. The model map function is explicitly quasiconformal: Topographic shear must be accounted for in V1, V2, and V3.

G2. Global anatomy is correct: The model must approximate the global shapes of V1, V2, and V3, as well as their relative surface areas, which are significantly different in the human and the macaque.

G3. Correct boundary conditions: Adjacent topographic areas must exhibit boundary conditions such that V1 and V2 share a boundary along the vertical meridian representation, and V2 and V3 share a boundary along the horizontal meridian representation.

G4. Mirror reflection around boundaries: The Jacobian determinant of the topographic map must reverse sign across the boundaries between V1, V2, and V3, exhibiting the *field reversal* property observed by Talbot (1942), Zeki (1969), and exploited by Sereno, McDonald, and Allman (1994), Sereno et al. (1995).

G5. V1 magnification factor is roughly inverse-linear in the foveal and parafoveal representations: Iso-eccentricity lines must be located approximately logarithmically with respect to the visual field eccentricity coordinate, in order to be consistent with previous studies. This means that inverse magnification factor is approximately linear. In the periphery (beyond 20°), the inverse magnification factor is super-linear, i.e., it rises more quickly in the periphery than in the central representations (Schwartz, 1983, 1984; Van Essen et al., 1984). A power-law fit (rather than a linear fit) to inverse eccentricity magnification factor over the full visual field was performed by Van Essen et al. (1984), resulting in an exponent of 1.11. This differs somewhat from the exponent of 1.00 corresponding to the monopole map, which accounts for only the foveal and parafoveal fields.

G6. Quantitative agreement with data: An error analysis of the two-dimensional model fit to existing data, although rarely present in topographic modeling studies, must be provided.

We now present the Wedge–Dipole model, which provides a unified model of V1, V2, and V3 that meets the stated goals G1–G6 above.

2.7. The Wedge–Dipole model

The Wedge–Dipole model accounts for the topographic structure of striate and extra-striate cortex by means of a *quasiconformal map function* that assigns coordinates of the spherical visual field to the two-dimensional cortical surface.

The mapping given by the Wedge–Dipole model results from constraining the map function to meet each of the stated goals for the topographic model. It consists of the composition of a (quasiconformal) wedge mapping with a (conformal) dipole mapping. A simple geometric account of the Wedge–Dipole model will be presented in terms of a series of illustrative figures. The mathematical details of the composite Wedge–Dipole mapping can be found explicitly in the first section of the Mathematical Appendix, and an algorithm for computing the Wedge–Dipole mapping is presented, in the form of executable code, in the second section of the Mathematical Appendix.

2.7.1. Projection of the visual field

In order to represent the spherical visual field as a planar model, we use an *azimuthal equidistant projection* of the hemisphere to the plane to produce the half-disc (Milnor, 1969). This projection identifies eccentricity as the radial coordinate in the plane and azimuth as the angular coordinate in the plane, resulting in a two-dimensional polar coordinate system representing the visual field. The azimuthal equidistant projection is a simple, closed-form near-isometric flattening method that maximally preserves the geometry of the original three-dimensional spherical surface (Milnor, 1969; Pearson, 1982). Any global coordinate parameterization of the visual field is acceptable, although, naturally, the parameters of any visual field mapping to the cortex will depend on the specific choice of visual field projection.

Also, we ignore the fact that the peripheral visual field does not conform exactly to a half-disc, but is a somewhat irregular shape, as indicated in classical perimetry (e.g., Inouye, 1909; Polyak, 1941). Were more quantitative peripheral data available, it would be straightforward to account for the non-circular full-field by masking the present model with the observed perimetric boundaries.

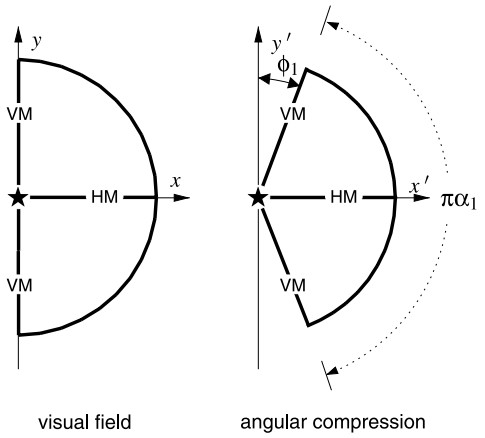

Fig. 3. The wedge mapping for V1 consists of an angular compression of the contralateral visual hemi-field by a factor of α_1 such that the visual hemi-field maps to a wedge-shaped representation of equal radius. The labels "HM" and "VM" mark the horizontal meridian and vertical meridian representations, respectively, and the "★" denotes the location of the foveal representation.

2.7.2. Wedge mapping V1

Fig. 3 illustrates the basic, non-conformal *wedge mapping*. A half-disc, representing the projected contralateral visual hemi-field, is mapped into a circular sector that we call a visual field "wedge," parameterized by the angular compression factor, α_1. This parameter is simply the reciprocal of the anisotropy index proposed by Van Essen et al. (1984). In geometrical terms, this mapping is accomplished by "squeezing" the angular polar coordinate of each point in the half-disc by an amount equal to the azimuthal shear, or, equivalently, by the reciprocal of the anisotropy index. This mapping is explicitly non-conformal—at each point, there is a different scaling applied in the radial and angular coordinate directions, thus the mapping is locally anisotropic.

2.7.3. Wedge mapping and mirroring V2

Fig. 4 shows a similar wedge mapping, parameterized by the angular compression α_2, applied to the contralateral visual field representation within V2. The four panels of the figure show:

1. A projected half-disc representing the contralateral visual hemi-field;
2. the wedge map of half-disc, with azimuthal shear parameter α_2;
3. mirror image of the wedge map with respect to the vertical axis; and
4. the wedge map split along horizontal meridian and rotated until the V1 and V2 vertical meridians are coincident.

Since V1 and V2 share boundary conditions along the vertical meridian, and since the contralateral visual hemi-field representation in V2 is a mirror image of the representation in V1 reflected across the vertical meridian, this construction is required. The goal is to provide a single domain that consists of multiple visual hemi-field projections, one for each of V1 and V2, with the correct boundary conditions. In the case of V1 and V2, this consists of forcing the vertical meridian representations to be coincident in the domain of the mapping. Then, since the map function and its inverse are presumed to be continuous, the meridians will also be coincident in the range, i.e., V1 and V2 will share the same cortical representation along the vertical meridian (cf. Gattass, Sousa, & Gross, 1988; Mallot, 1985).

Note that the V2 wedge mapping can be easily extended to allow for independent values for the constant azimuthal shear in the upper and lower quadrants of the visual hemi-field. This simple generalization is useful when describing data that exhibits asymmetric visual field representations in dorsal and ventral V2.

A very similar process is applied to incorporate V3 into the wedge complex, but this time mirroring with respect to the V2 representation of the horizontal meridian, since V2 and V3 meet at a shared horizontal meridian representation.

2.7.4. The wedge map composed with the dipole map

Fig. 5A shows three copies of the (projected) visual hemi-field, represented as half-discs. They are mapped into individual wedges, mirrored, and re-aligned, and finally combined into a single wedge complex in Fig. 5B. The final cortical image—the dipole complex obtained by applying a dipole map to the wedge complex—is shown in Fig. 5C.

The formulation of the Wedge–Dipole model in terms of three copies of the visual field being mapped in parallel into visual cortex was chosen for its simplicity. However, a hierarchical conceptualization in which the visual field representation first maps into V1, then the V1 representation is mapped directly into V2, and V2 into V3, is the actual biological realization. It is straightforward to formally express the V1–V2–V3 Wedge–Dipole mappings in a hierarchical or feed-forward form by properly composing combinations of the wedge and dipole maps and their inverses, but the resultant expressions are far more complicated.

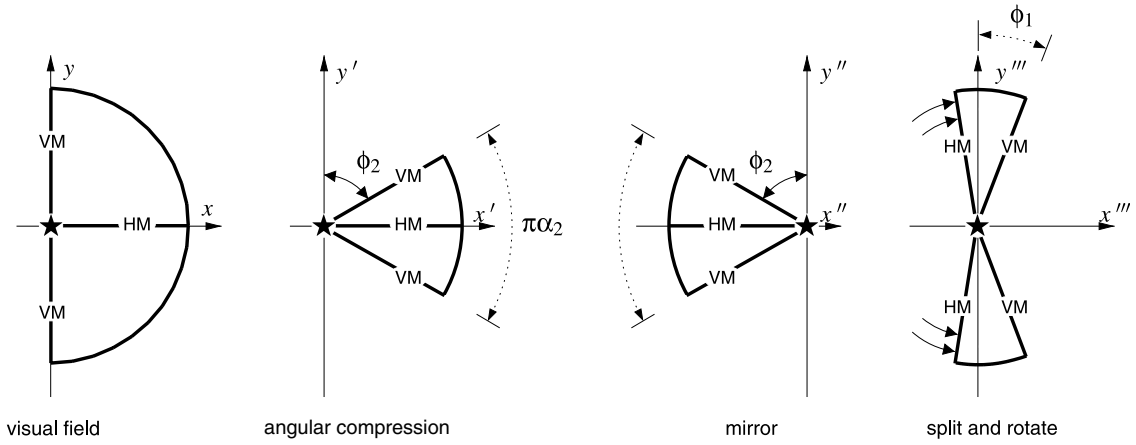

Fig. 4. The wedge mapping for V2 requires extra steps to induce the field reversal and to meet the boundary condition imposed by V1. The angular compression of the contralateral visual hemi-field by the factor of α_2 maps the visual hemi-field into a wedge-shaped representation of equal radius. Then, the wedge is mirrored about the y axis. Finally, the compressed wedge is split along the horizontal meridian representation into half-wedges representing the upper hemi-field and lower hemi-field, which are then each rotated away from the negative x axis until the vertical meridian representation aligns with that of the V1 wedge, shown in Fig. 3. Note that the angle ϕ_1 represents the angle between the vertical meridian representation and the y axis in the V1 wedge map. The labels "HM" and "VM" mark the horizontal meridian and vertical meridian representations, respectively, and the "★" denotes the location of the foveal representation.

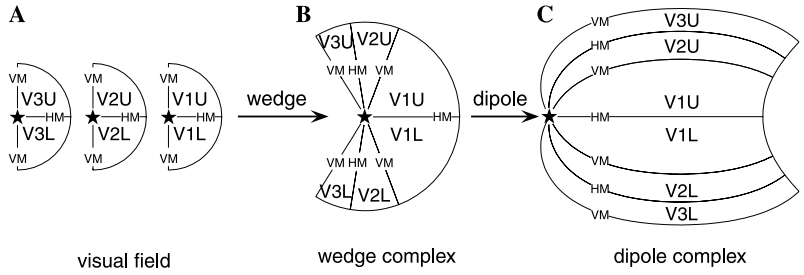

Fig. 5. Schematic of the mapping composition. (A) Three copies of the contralateral visual field (one each for V1, V2, and V3) are mapped into the wedges shown in (B) by the wedge map. The dipole map is then applied to the wedges, resulting in the full Wedge–Dipole map, shown in (C). The "★" denotes the location of the foveal representation. The quadrants of each visual hemi-field are labeled as "V1U," "V2U," and "V3U" for the upper field, and "V1L," "V2L," and "V3L" for the lower field. The horizontal meridian and vertical meridian are labeled as "HM" and "VM," respectively.

A useful feature of the Wedge–Dipole construction is that since the dipole mapping is conformal and, therefore, introduces no shear, the total shear in the composite mapping is equal to the shear in the wedge mapping. Thus, we can fully characterize the shear in each cortical topographic area with the corresponding azimuthal shear parameter α.

We can summarize the Wedge–Dipole mapping via two main points.

1. The wedge mapping takes three copies of the visual hemi-field, and compresses them azimuthally, mirrors, and combines them to construct a single domain with the correct boundary conditions and azimuthal shear.
2. A *single* dipole map, applied to this composite domain, provides the final cortical layout of V1, V2, and V3.

The previous figures have focused on illustrating the mapping of the *boundaries* of V1, V2, and V3. Figs. 6 and 7 illustrate the combined wedge and dipole map for the iso-eccentricity and iso-azimuth lines as well. These diagrams emphasize the continuous nature of the V1–V2–V3 complex, in the sense that the cortical representation of all three areas can be viewed as a single map complex, relative to the domain represented by the wedge complex. Additionally, each diagram depicts the mapping of the upper visual hemi-field to the ventral half and the lower visual hemi-field to the dorsal half of the dipole complex.

Thus far, the Wedge–Dipole model has been shown to achieve the first five goals outlined above.

G1. The model map function is explicitly quasiconformal: The wedge map imposes a constant compressive shear in the azimuth direction. This results in a compression along the iso-eccentricity contours of the dipole map, inducing a simple form of shear in each of the areas of the Wedge–Dipole map.

G2. Global anatomy is correct: The dipole parameters a and b determine the overall shape of the area borders, and the compression parameters α_1, α_2, and α_3 not only prescribe the shear, but also allow the relative surface areas to be varied to match the data.

G3. Correct boundary conditions: The wedge map construction enforces the boundary conditions between adjacent areas—image points of the V1 vertical meridians correspond to image points of the V2 vertical meridian, and likewise image points of the V2 horizontal meridians correspond to image points of the V3 horizontal meridians.

G4. Mirror reflection around boundaries: Since the mapping derivative in the iso-eccentricity direction reverses sign across the V1–V2 boundary and V2–V3 boundary, the Jacobian determinant of the Wedge–Dipole map reverses sign across the borders of adjacent areas.

G5. V1 magnification factor is roughly inverse-linear in the foveal and parafoveal representations: By construction, the dipole mapping ensures logarithmic spacing of iso-eccentricity lines, with a super-linear inverse magnification factor in the peripheral representation.

The quantitative agreement with data required for goal *G6* is demonstrated below.

3. Results

The Wedge–Dipole model provides a good qualitative fit to the estimated topography of visual areas V1, V2, and V3 in human provided by Horton and Hoyt (1991a) and estimates of owl monkey topography in V1 and V2 provided by Allman and Kaas (1975), as demonstrated in Figs. 8 and 9, respectively. However, these data are semi-quantita-

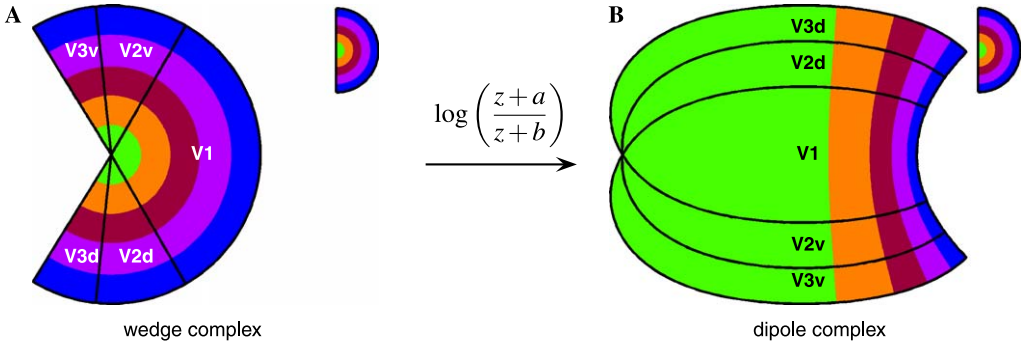

Fig. 6. Schematic visual field eccentricity mapping into the wedge complex and the dipole complex. (A) The eccentricity of the visual field for the combined wedge complex for V1, V2, and V3 demonstrates that the azimuthal compression induced by the wedge mapping changes the azimuth but does not affect eccentricity. The representation of eccentricity is also shown to be continuous across the region boundaries. (B) The visual field representation in cortical space, after applying the dipole mapping to the wedge complex. The eccentricity of the internal topographic representation demonstrates the magnification of the foveal representation as well as the compression of the periphery in all three regions shown. Additionally, the iso-eccentricity bands are shown to intersect each region boundary orthogonally and to be continuous across the boundaries. The half-disc inset in the upper right of each panel provides the eccentricity on the visual hemi-field in pseudocolor.

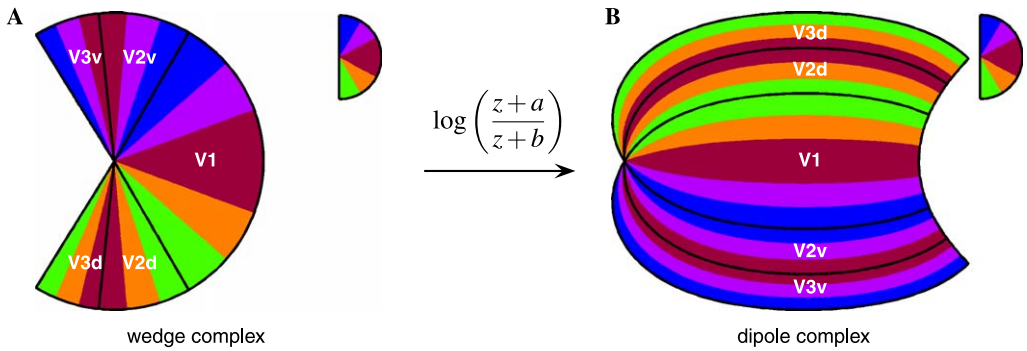

Fig. 7. Schematic of the visual field azimuth mapping into the wedge complex and the dipole complex. (A) The azimuth of the visual field for the combined wedge complex consists of the wedge mappings of V1, V2, and V3, demonstrating the azimuthal compression of the visual field as well as the field reversal across wedge boundaries. (B) The outcome of applying the dipole mapping to the wedge complex shows the field reversal property in cortical coordinates: across any given border between two cortical regions the direction of increasing azimuth reverses. The V1/V2 border represents the vertical meridian of the visual field, whereas the V2/V3 border represents the horizontal meridian, resulting in the the *ventral half* of the cortical space representing the upper quadrant of the visual field and the *dorsal half* representing the lower quadrant. The labels "V2v" and "V3v" indicate the ventral halves of V2 and V3, and "V2d" and "V3d" indicate the dorsal halves. The half-disc inset in the upper right of each panel provides the azimuth on the visual hemi-field in pseudocolor.

tive estimates of topography. Although they were essential to the formulation and development of the Wedge–Dipole model, they are ultimately inadequate for quantitative modeling. In this section, we demonstrate quantitative, two-dimensional model fits to two independent sets of macaque visual topography data.

3.1. 2DG labeling of macaque V1

To obtain an accurate characterization of the two-dimensional topographic mapping in macaque V1, we first fit the standard monopole model to previously published, two-dimensional *macaca fascicularis* visual topography data in the form of 2DG-labeled V1 activation evoked

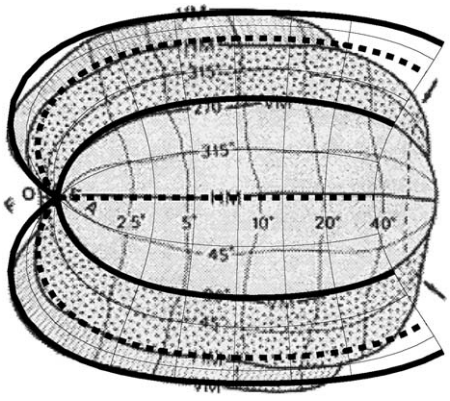

Fig. 8. The topography of human visual areas V1, V2, and V3 from Horton and Hoyt (1991a) (as shown in Fig. 1) with the iso-eccentricity and iso-azimuth contours predicted by the Wedge–Dipole model superimposed on the three areas. The model parameters used here were $a = 0.9°$, $b = 180°$, $\alpha_1 = 0.95$, $\alpha_2 = 0.5$, and $\alpha_3 = 0.2$. The value of a here is somewhat higher than we have found for quantitative analysis of macaque and human, possibly due to the semi-quantitative nature of this data set. The representation of the horizontal meridian in the Wedge–Dipole model is shown with thick dashed lines, and the representation of the vertical meridian is shown with thick solid lines.

during presentation of a visual stimulus (Schwartz, 1994; Schwartz et al., 1989a). In this experiment, the stimulus consisted of spatially static, logarithmically spaced rings, and uniformly spaced rays together with square textured figures, which were flashed in counter-phase on a computer monitor. This data set is unique in that it contains visual topography data for both hemispheres of one subject and the two hemispheres were each processed differently. The activity patterns seen in the flattened cortex from both hemispheres, along with the visual stimulus pattern, are shown in Fig. 10B.

The surface representing the full extent of macaque V1 from the left hemisphere was reconstructed from serial coronal tissue sections and the 2DG-labeled activity pattern from layer IV was texture mapped onto a near-isometric flattening (Schwartz et al., 1989b) of the V1 surface mesh. The reconstructed three-dimensional surface consisted of 2125 triangle faces composing 804 mm^2 of surface area. The surface flattening exhibited a weighted root-mean-square (RMS) error of 13.3% (Balasubramanian, Polimeni, & Schwartz, 2005). (The *weighted RMS error* is an RMS error measure adjusted for non-uniform spacing of mesh vertices on the surface.)

The data from the right hemisphere, in contrast, consist of the opercular cortex physically flattened between glass cover slips, cut tangentially through layer IV, and processed for 2DG autoradiography. The surface area of the flattened tissue was about 400 mm^2. The peak metric error introduced by this physical flattening procedure applied to macaque opercular cortex has been demonstrated to be at least 30% (Schwartz et al., 1989b), with considerably larger errors expected for physical flattening applied to the full macaque V1 or to additional tissue from extra-striate areas. For this reason, we do not fit our quantitative model to the topography data of the hand-flattened V1.

However, the availability of both hemispheres from the same individual provides the unique ability to directly

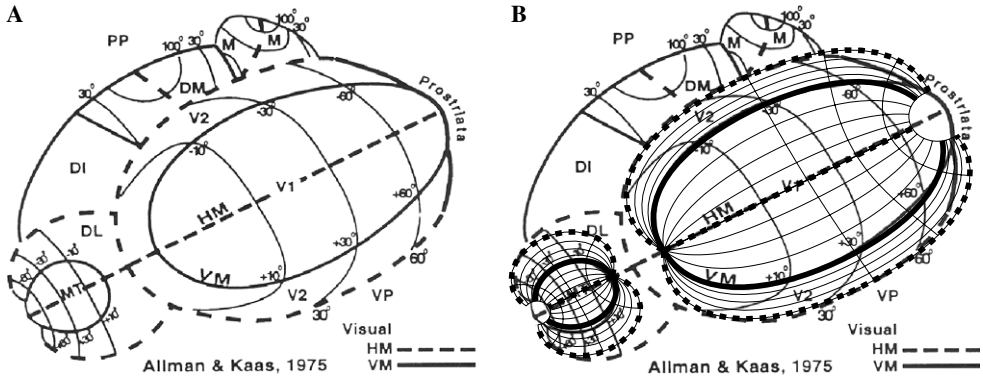

Fig. 9. The topography of owl monkey visual cortex is shown in (A) from the data of Allman and Kaas (1975) (reproduced from Kaas, 1997, chap. 3). Two Wedge–Dipole maps are shown superimposed on this data set in (B), one for the V1–V2 complex (model parameters $a = 0.8°$, $b = 85°$, $\alpha_1 = 1.05$, and $\alpha_2 = 0.33$), and one for the MT–DL complex (model parameters $a = 10°$, $b = 70°$, $\alpha_1 = 1$, and $\alpha_2 = 0.5$). The MT–DL model has been scaled by a factor of 0.65 relative to the V1–V2 model. "HM" and "VM" mark the cortical representation of the horizontal meridian and vertical meridian, respectively, in the data. The representation of the horizontal meridian in the Wedge–Dipole model is shown with thick dashed lines, and the representation of the vertical meridian is shown with thick solid lines.

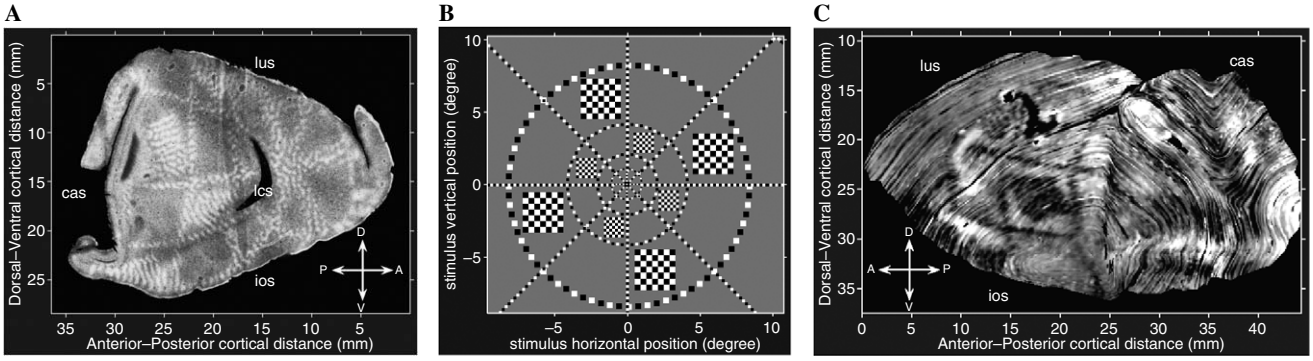

Fig. 10. (A) Visuotopy data obtained from tangential section through layer IV of physically flattened macaque V1 of right hemisphere. (B) The visuotopic mapping stimulus consisted of a ring and ray pattern of black-and-white checks and subtended approximately 20° of the visual field. (C) Near-isometrically flattened computer reconstruction of macaque V1 visuotopy data from the left hemisphere of the same macaque. The local coordinate directions for the opercular cortex are given in the legend. *Abbreviations: cas*, calcarine sulcus; *lus*, lunate sulcus; *ios*, inferior occipital sulcus; and *lcs*, lateral calcarine sulcus.

validate measurements of the fixational offset and cyclotorsion exhibited by the paralyzed eye, which resulted in a displacement of the stimulus origin from the center of the fovea. In this experiment, the stimulus was presented monocularly to the right eye, and the activity pattern corresponding to the center of the stimulus pattern can be clearly seen in the right hemisphere data shown in Fig. 10A. The eye offset was estimated to be 1° to the right of the stimulus origin with an 11° counter-clockwise rotation relative to the stimulus reflecting the combination of paralysis-induced eye intorsion and residual rotation with respect to the stimulus display (Schwartz, 1994).

In the original study of this data set, the computer-flattened data were fit to a numerical conformal mapping to test the conformality of the visuotopic mapping function (see Schwartz, 1994). The conclusions from the original study were that the mapping exhibited strong local isotropy and closely resembled the standard monopole model. For the present study, we directly tested the fit of the monopole model to the data and used the model to characterize the two-dimensional topographic mapping. To do this, features of the visual stimulus in the 2DG-labeled data were identified and the monopole model was fit to the data using these point correspondences. The point correspondences between the stimulus and activity pattern in V1 are presented in Fig. 11 for the reconstruction of V1 from the left hemisphere.

To optimize the fit of the monopole model to the data, we first constructed an error measure that quantifies the model fit. Let (x_j,y_j) be the Cartesian coordinates of vertex j in the flat map shown in Fig. 11B. The eccentricity and azimuth of the point P_j in the visual field corresponding to this vertex are specified in the 2DG data, and can therefore be used to compute the mapping of P_j to a point $(\hat{x}_j,\hat{y}_j)$ in cortex via the monopole model, given a particular choice of model parameters. In other words, the monopole model *predicts* that P_j will map to a point in cortex with Cartesian coordinates $(\hat{x}_j,\hat{y}_j)$, whereas the *measurements* indicate that P_j maps to a point in cortex with coordinates (x_j,y_j). Therefore, the displacement between (x_j,y_j) and

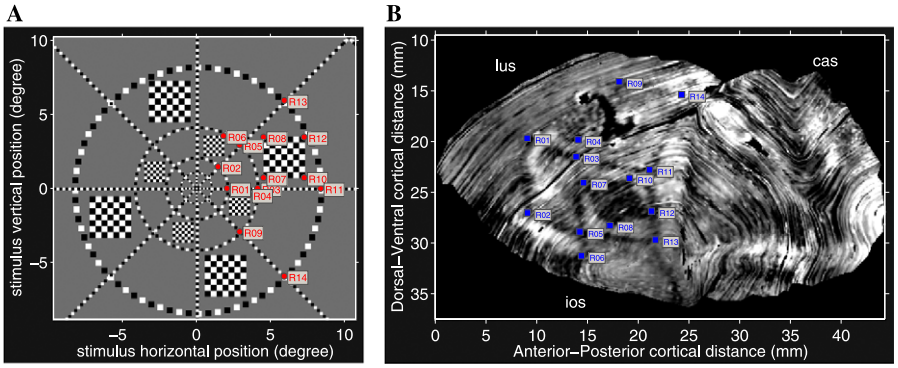

Fig. 11. (A) The numbered red circles mark features of the visual stimulus within the right hemi-field identified in the 2DG labeling of V1 that were used for the model fit. (B) Computer reconstruction of V1 from the left hemisphere. The 2DG-labeled activity pattern from layer IV was texture mapped onto numerically flattened V1 surface mesh. The numbered blue squares correspond to the locations of the visual stimulus features shown in (A).

$(\hat{x}_j, \hat{y}_j)$ provides a measure of the error between the data and the model for any given vertex j. Let d_j be the (Euclidean) magnitude of this displacement—that is,

$$d_j = \sqrt{(\hat{x}_j - x_j)^2 + (\hat{y}_j - y_j)^2}. \quad (1)$$

The RMS value of d_j was chosen as an error measure, E_{RMS}, over the entire mesh. The RMS displacement error is given by

$$E_{\mathrm{RMS}} = \sqrt{\frac{1}{N}\sum_{j=1}^{N} d_j^2}. \quad (2)$$

Note that E_{RMS} depends (via $\hat{x}_j$ and $\hat{y}_j$) on the monopole parameter a as well as the global scale (i.e., parameter k), rotation, and translation of the cortical map. The Nelder–Mead Simplex algorithm (Lagarias, Reeds, Wright, & Wright, 1998; Nelder & Mead, 1965) was used to minimize E_{RMS}, resulting in best-fitting parameter values for the monopole model of $a = 0.72°$ and $k = 8.72$ mm/° for the 14 usable stimulus features from the near-isometric flattening of the left hemisphere. (The implementation of the Nelder–Mead Simplex algorithm used for this study was the implementation in MATLAB 6.1, i.e., the function `fminsearch`.)

To ensure that these parameter values reflected the global minimum of the RMS error function, several trials of the optimization were computed each with a randomly chosen set of initial conditions for the parameter values. This procedure provides a measure of the parameter value error attributable to the fitting method. However, in all trials the resulting parameter values were identical, indicating that these parameter values provide the global optimum for our figure-of-merit function.

The resulting monopole fit is presented in Fig. 12. Fig. 12A shows the residual errors between the measured and predicted positions as well as the estimated projection of the rings and rays of the visual stimulus. The measurements and model predictions are in excellent agreement. The resulting median error is 0.95 mm, the mean error is 0.95 mm, and the RMS error is 1.07 mm. Taken as a percentage of the size of V1, the relative RMS error is about 3%.

Another measure of the ability of the model to fit the data can be constructed by considering how well x_j and

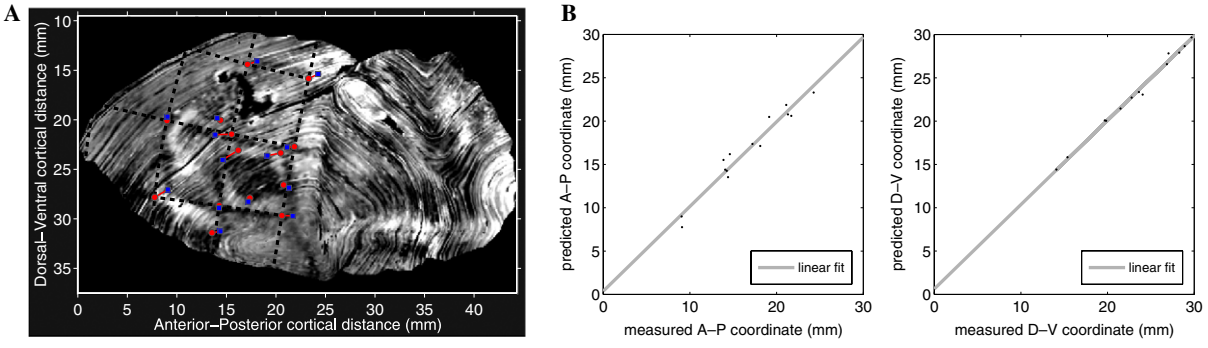

Fig. 12. Monopole model fits to computer-reconstructed macaque visuotopy. (A) Comparison between optimal model fit and data. The model parameters were obtained by minimizing the RMS error between the model prediction and the data. The blue squares mark the data points, the red circles mark the model prediction for each data point, and the red line segments connect corresponding measurement-prediction pairs. The black dashed lines represent the predicted locations of the rings and rays of the visual stimulus, which match the imprinted representation of the stimulus in the data well. (B) Plot of the measured versus predicted coordinate values for each data point. The correlation coefficient for the position along the anterior–posterior axis and the position along the dorsal–ventral axis was 0.98 and 0.99, respectively, indicating that the model was able to account for the variance in the data and thus provided a good fit.

y_j correlate with $\hat{x}_j$ and $\hat{y}_j$. These correlations between the measurements and the model predictions, shown in Fig. 12B, were extremely high, indicating that the model was able to account for the variance in the data and thus provided a good fit.

Given the relatively small number of data points comprising this data set, and the existing demonstration of global visuotopic conformality of this data set (Schwartz, 1994), we chose to fit the conformal monopole model to the data rather than a model with topographic shear since the conformal monopole model requires fewer parameters. To test whether a quasiconformal generalization of the monopole model could provide a better fit to the data at the expense of an additional parameter, we also fit the data to a mapping given by the *Wedge–Monopole* model—that is, a monopole mapping composed with a wedge mapping that introduces azimuthal topographic shear parameterized by α_1 as described in Section 2. The Wedge–Monopole fit produced parameter values $a = 0.78°$, $k = 8.95$ mm/°, and $\alpha_1 = 0.98$, with an RMS fitting error of 1.07 mm. The a and k parameter values are virtually identical to those produced by the monopole fit. Surprisingly, the RMS errors exhibited by the fits to the two models were identical despite the additional degree of freedom possessed by the Wedge–Monopole model granted by the shear parameter α_1. Since the value of the constant azimuthal shear parameter α_1 is nearly unity, the quasiconformal generalization of the monopole mapping is unwarranted in this case: the conformal monopole mapping suffices. To confirm that the addition of the shear parameter α_1 does not reduce model prediction error for this data set, we calculated the "leave-one-out" or N-fold cross-validation error (Hastie, Tibshirani, & Friedman, 2001), where N is the number of data points, for both model fits. As with the RMS fitting error, the cross-validation error was identical (0.98 mm) for the two models, indicating that the constant azimuthal shear parameter α_1 is redundant for describing the topographic mapping of this data set. We believe that the negligible shear demonstrated by the 2DG data may be due to the concentration of the usable image features in the general region of the horizontal meridian representation, with a consequent under-representation of the region containing the vertical meridian representation where independent evidence suggests that the shear is largest.

These measurements of macaque topography provided by the monopole model offer a two-dimensional characterization of the V1 topography based on the central-field topography of V1 alone, supplying an initial estimate of the monopole model parameters a and k. A much more extensive data set, including data from the visual field periphery, is required to fit the full set of Wedge–Dipole parameters. Fortunately, there is a publicly available data set of this form that consists of measured and estimated topographic markers on a cortical surface mesh, enabling the application of accurate brain flattening algorithms to represent the topographic data in the plane. This data set is analyzed in the next section.

3.2. Full-field macaque V1–V2 electrophysiology data

Quantitative topography data gathered from extensive microelectrode recordings has been made publicly available by D. C. Van Essen and colleagues (see http://brainmap.wustl.edu/). In particular, one of the available data sets (atlas F99UA1) provides a triangular mesh reconstruction of the right hemisphere of macaque cerebral cortex, along with the corresponding values of visual field eccentricity and azimuth for each vertex in V1 and V2; there was no V3 topographic data provided with this atlas. Fig. 13 shows two views of V1 and V2 from this data set, with several iso-eccentricity and iso-azimuth lines overlaid on the surface.

The V1 topography data in this data set originated from a study by Van Essen et al. (1984). V2 topography was mapped onto the atlas using an additional data set, where the topography data were estimated using a combination of anatomical connectivity information (between V1 and V2) and physiological mapping (Van Essen, Felleman, DeYoe, Olavarria, & Knierim, 1990).

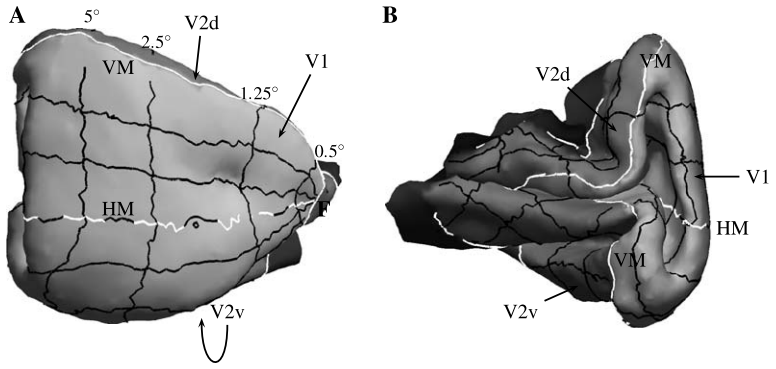

Fig. 13. (A) A lateral view of V1 (light gray) and V2 (medium gray) of macaque visual cortex. (B) A medial view of V1 and V2, exposing the calcarine sulcus. Several iso-eccentricity and iso-azimuth contours are shown (as solid lines) on the cortical surface. "HM" (dashed white line) and "VM" (solid white line) mark the cortical representation of the horizontal meridian and vertical meridian, respectively, and "F" marks the representation of the fovea. "V1" marks striate cortex, and "V2d" and "V2v" mark dorsal and ventral V2, respectively. The topography of V1 and V2 is easier to visualize on a flattened representation of these areas, as shown in Fig. 14A.

The mesh shown in Fig. 13, representing the cortical surface within areas V1 and V2, was flattened using the DMflatten near-isometric flattening algorithm (Balasubramanian et al., 2005), yielding a weighted RMS error of 19.2%. The resulting flattened cortical surface is shown in Fig. 14A. From this figure, it can be seen that ventral V2 (which contains a representation of the upper visual hemi-field) appears to be much larger in surface area than dorsal V2. To account for this asymmetry, we extended the model to incorporate two shear parameters for V2, α_2^V and α_2^D, which can be adjusted independently to match the area of each half of V2 (see Mathematical Appendix for model equations). This replaces the original V2 uniform shear parameter α_2 with two different uniform shear parameters α_2^V and α_2^D for the upper and lower visual quarter-field representations in this hemisphere, respectively. In other words, α_2^V is the azimuthal shear for ventral V2 and α_2^D is the azimuthal shear for dorsal V2.

The optimization procedure for computing the best-fitting parameters was identical to that described in Section 3.1, except that here the Wedge–Dipole model is fit to the full-field V1 and V2 F99UA1 data. Thus, E_{RMS} now depends on the wedge map parameters α_1, α_2^V, and α_2^D; the dipole parameters a and b; and the global scale, rotation, and translation (see Mathematical Appendix). The resulting best-fitting parameter values for the asymmetric Wedge–Dipole model were $a = 0.75°$, $b = 76.8°$, $\alpha_1 = 0.78$, $\alpha_2^V = 0.55$, and $\alpha_2^D = 0.49$.

The measurement of Wedge–Dipole parameter a, which characterizes the percentage of macaque visual cortex devoted to representing the central visual field, is based on data compiled from the full visual field as well as both areas V1 and V2, but is in good agreement with the measurements made from the 2DG data presented in Section 3.1 that are based on central-field data from V1 alone.

The resulting global azimuthal shear ratio measured in V1 is in agreement with the supra-columnar V1 anisotropy of $\alpha_1 = 0.66$ near the vertical meridian and $\alpha_1 = 0.87$ near horizontal meridian, reported by Blasdel and Campbell (2001), and in disagreement with the hypothesis for V1 columnar-topographic relationships of Tootell et al. (1988). Our results for V2 shear are in strong disagreement with the hypothesized supra-columnar anisotropy of $\alpha_2 = 0.16$ suggested by Roe and Ts'o (1995). Their hypothesis is based on extrapolation of sub-columnar measurements via a hypothesis of how these relate to global topography. This hypothesis is identical in concept to that proposed for V1 topography by Tootell et al. (1988), and leads to V2 global shear which is many times larger than that observed in the data. However, our results agree more with both the experimental observations of Rosa et al. (1988) in cebus monkey and of Shipp and Zeki (2002) in macaque, who reported a V2 anisotropy of $\alpha_2 = 0.58$–0.66 based on direct, supra-columnar measurements.

The Wedge–Dipole model with our optimized parameter settings is shown in Fig. 14B, along with the displacement between the measured location and the predicted location of the image of a few points in the visual field. A histogram of the errors d_j is shown in Fig. 14C. The cross-validation error is 2.4 mm, the median error is 2.1 mm, the mean error is 2.4 mm, and the RMS error is 2.9 mm, which is about 5% of the width of V1–V2 (approximately 60 mm for the F99UA1 macaque).

The resulting correlation coefficient quantifying how well x_j correlates with $\hat{x}_j$, r_x, is 0.98 for the resulting fit. Similarly, we obtain a correlation coefficient $r_y = 0.99$ for the correlation of y_j with $\hat{y}_j$ (see Fig. 15). Computing the r^2 statistic, we obtain $r_x^2 = 0.97$ for the x-coordinate and $r_y^2 = 0.98$ for the y-coordinate. This statistic tells us that the model accounts for over 97% of the variance of x- and y-coordinates of the vertices.

From Fig. 14B it can be seen that the Wedge–Dipole model fits the data well, with the larger errors located at the cortical representation of the fovea and the far periphery. It is interesting to note that these regions are

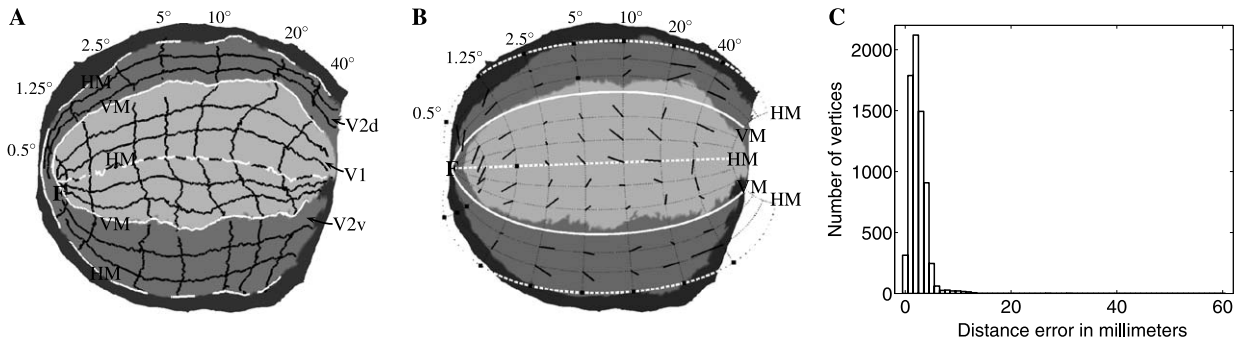

Fig. 14. (A) Near-isometric flattening of macaque V1 (light gray) and V2 (medium gray), with several iso-eccentricity and iso-azimuth contours shown as black lines. "HM" and "VM" mark the cortical representation of the horizontal meridian and vertical meridian, respectively, and "F" marks the representation of the fovea. "V1" marks striate cortex, and "V2d" and "V2v" mark dorsal and ventral V2, respectively. (B) The corresponding iso-eccentricity and iso-azimuth contours are shown (as dotted lines) for a fit of the Wedge–Dipole map to the data in (A). The model parameters were obtained by minimizing the RMS value of the error per vertex. The short black line segments indicate displacements from the intersections of the iso-eccentricity lines with the iso-azimuth lines in the model to the corresponding locations in the data in (A). The black squares correspond to locations where the lines in (A) do not intersect due to missing data. (C) A histogram of modeling errors (i.e., distances between the data and the model predictions).

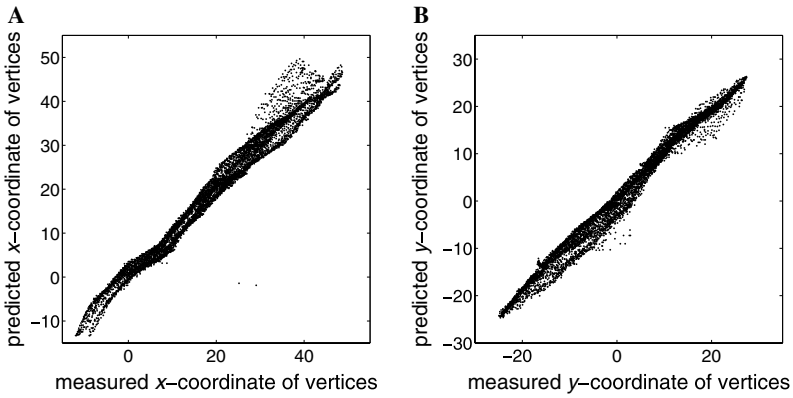

Fig. 15. The results of minimizing the RMS error of the Wedge–Dipole model fit to V1 and V2 topography in the F99UA1 data set. The cortical coordinates of the data points plotted against model predictions for (A) the x coordinate and (B) the y coordinate.

the ones in which it is most difficult to collect accurate visuotopic data: close to the foveal representation, uncertainties in eye fixation result in large displacement errors in cortex, and in the far periphery, it is technically difficult to collect precise spatial data due to large receptive field size.

Note that the F99UA1 topography data were constructed by registering V1 topographic data from one study (Van Essen et al., 1984) to V2 topographic data from a separate study (Van Essen et al., 1990). As uncertainties arise in each stage of registration, it is not clear how much of the error we have reported for the model fit is simply due to errors in the registration process.

4. Discussion

4.1. Possible extensions of the Wedge–Dipole model

4.1.1. Removal of "pinch" in foveal representation

One characteristic of the Wedge–Dipole model is that the foveal representations of V2 and V3 meet V1 at a single point, as shown in Fig. 5. Although little data are available concerning the foveal representation of V1, V2, or V3, it is possible that the foveal representation in V2 may extend beyond the V1 representation before the horizontal meridian representation bifurcates, as demonstrated in Fig. 1.

To examine this possibility, we considered an *eccentric power function*, similar to that used by Mallot (1985) as a component in a model of the topographic mapping of areas 17, 18, and 19 of cat visual cortex. The eccentric power function consists of a simple translation of the V1–V2 wedge complex, followed by an exponentiation, which together require two additional parameters. This auxiliary mapping results in a modified wedge complex whose foveal representation in V2 extends away from the foveal representation of V1. When this modified wedge complex is transformed by the dipole mapping, the effect is to alleviate the "pinch" at the foveal representation, thus we refer to this new modification as "unpinching" the V2 foveal representation. Example unpinched wedge and dipole complexes

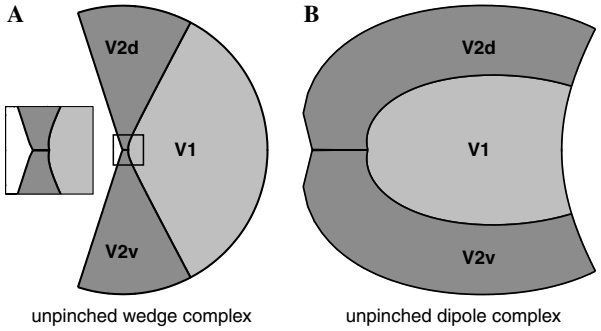

Fig. 16. (A) "Unpinching" the wedge complex consists of moving the complex to the right of the origin then bending the complex around the origin. The inset shows a close-up of the unpinched wedge complex at the foveal representation. (B) The result of mapping the unpinched wedge complex through the dipole mapping is a dipole complex in which the the foveal representation in V2 assumes more cortical area (cf. Fig. 1).

appear in Fig. 16, and the mathematical description of this unpinching map is presented in the Mathematical Appendix.

Although this modification provides a reasonable extension to the area of the V2 foveal representation, the lack of quantitative foveal data obstructs detailed exploration of spatial mapping in the region of the foveal confluence at the present time.

4.1.2. The monocular crescent

The boundary of the peripheral visual field representation in V1 predicted by the dipole mapping is clearly *concave*—in Fig. 2, one can see a "notch" missing in the peripheral representation corresponding to the furthest extent of the visual half-disc under the mapping. However, it has been observed anatomically that the peripheral border of V1 is not concave but rather appears flat, resulting in a *convex* border for V1.

Interestingly, the border between binocular and monocular V1 situated in the peripheral visual hemi-field representation is also concave (see, e.g., Adams & Horton, 2003b; Horton, Dagi, McCrane, & de Monasterio, 1990; Horton & Hocking, 1996). This can be explored by

adopting a more realistic visual hemi-field geometry that includes both the binocular and monocular components of the visual hemi-field. Fig. 17A demonstrates a more realistic visual hemi-field perimeter that includes an explicit monocular region (cf. Inouye, 1909; Polyak, 1941). Under the dipole mapping, the cortical representation of the monocular visual field occupies the area of V1 that is the anatomical region known as the *monocular crescent*, as is shown in Fig. 17B.

As with the foveal confluence, we do not yet possess detailed information about the monocular and binocular visuotopy in the peripheral representations in visual cortex. Therefore this extension of the Wedge–Dipole model is merely a suggestion to account for the observed anatomical boundaries.

4.1.3. Non-uniformity in azimuthal shear

Thus far, we have assumed a constant azimuthal shear for the Wedge–Dipole mapping that has induced parameterized topographic anisotropy along the iso-eccentricity contours, based on reports that the compression of the visuotopic map in V1 is aligned parallel to the iso-eccentricity contours (see, e.g., Blasdel & Campbell, 2001; LeVay et al., 1975; Tootell et al., 1988).

Recently, Blasdel and Campbell (2001) have reported that the visuotopic anisotropy in macaque V1 is larger close to the V1–V2 boundary, and that the map is more nearly isotropic along the internal horizontal meridian representation [see also Adams and Horton (2003b) for similar results in squirrel monkey V1]. A first attempt at accommodating these observations is to use a slightly more complicated form of azimuthal compression—one that induces larger anisotropy near the V1–V2 boundary, falling to smaller values near the representation of the horizontal meridian. Fig. 18 demonstrates the results of applying a simple shear heuristic that unevenly spaces iso-eccentricity contours by introducing a single additional "shear non-uniformity" parameter for each topographic area that causes the azimuthal shear to be a sigmoidal function of azimuthal distance from the vertical meridian.

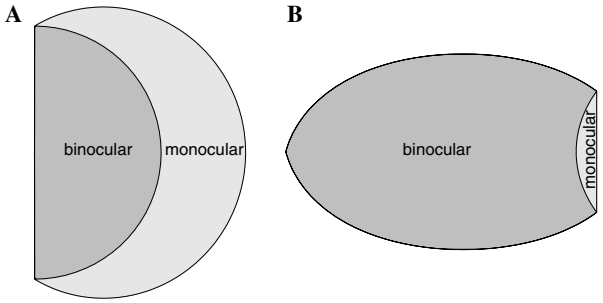

Fig. 17. Representation of monocular component of the visual hemi-field in V1 under the dipole mapping. (A) A qualitative model of the right visual hemi-field, with the monocular and binocular fields demarcated (cf. Polyak, 1941). (B) The representation of both the binocular and monocular visual hemi-field components in primary visual cortex under the Wedge–Dipole mapping. The outline of the monocular field representation, appearing in the peripheral area of V1, fills in the concave gap in the dipole mapping and resembles the anatomical shape of the monocular crescent.

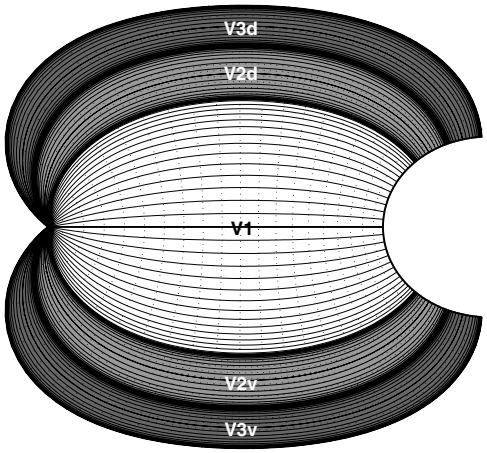

Fig. 18. Wedge–Dipole model with alternate azimuthal shear distribution. This extension includes a non-uniformity in the azimuthal shear term that induces greater azimuthal shear along the area boundaries. V1 is shown in light gray, V2 in medium gray, and V3 in dark gray. The solid lines internal to the areas represent the iso-azimuth contours of the visuotopic mapping, and the dotted lines represent the iso-eccentricity contours. The shear non-uniformity manifests as a tighter spacing of the iso-azimuth contours near the area boundaries (cf. Fig. 2C). The particular non-uniformity shown here corresponds to a sigmoidal compression near to the boundaries and expansion in the interior.

As with the unpinching map introduced in the previous section, we currently do not have access to sufficiently precise topographic data to quantitatively characterize shear in V1 more accurately, and, therefore, to evaluate more sophisticated shear models such as the one illustrated in Fig. 18. We conclude that the uniform-shear Wedge–Dipole model provides a simple, first-order model that works well for currently available data. Extensions to more realistic forms of shear, along the lines of the previous discussion, may, in the future, be easily incorporated into this model if more extensive data are available. In particular, as the topographic shear function becomes increasingly detailed and complicated, it would become efficient to simply resort to a numerical, as opposed to a closed-form, model. Methods for numerical quasiconformal modeling are briefly outlined below.

4.2. Conformal and quasiconformal models

4.2.1. Near-conformal case

To the extent that we can conceptualize the topographic structure of visual cortex in terms of a continuous map, strong mathematical constraints impose themselves on the data. First, any regular (i.e., quasiconformal) map can be decomposed into a term that is locally the sum of a conformal map and a shear map (Ahlfors & Bers, 1960; Segel, 1977).

If the shear component is small on average, as seems to be the case for macaque V1, then, without doubt, a conformal map of the data provides the simplest description. This is because conformal maps have powerful numerical attributes—the boundary or "shape" of V1 in addition to a *single* corresponding point between the visual hemi-field and cortex determine the entire map. This statement follows from the classical Riemann Mapping Theorem (Ahlfors, 1966a), and has been used to statistically characterize the accuracy of 2DG topography data via the Symm algorithm (a standard numerical algorithm for computing conformal mappings; see Kythe, 1998; Symm, 1966) using a jackknife replication technique (Schwartz, 1994). Briefly, a collection of retino- or visuo-cortical correspondences can be used, one at a time, to fix the conformal map model. Repeating this for each point in turn (i.e., performing jackknife replication) provides an estimate in the error of the conformal assumption, as has been previously performed on the flattened 2DG data presented in Fig. 11. The results suggest a conformal approximation for V1 which has an accuracy of 10–20% (Schwartz, 1994). The Riemann Mapping Theorem motivates this analysis, since it guarantees that the entire (conformal) topographic map reduces to a three-parameter fit (a single point correspondence and an orientation).

4.2.2. Simple global shear functions

If the shear function can be modeled as a constant global shear represented by a single parameter, then an almost equally favorable situation holds. As discussed above, it is a mathematical fact that all regular maps are locally the sum of a conformal and shear component. It is shown in the present report that this can be extended globally, writing the multi-area visuotopic map in terms of separate conformal (dipole) and shear (wedge) constructs. This is an enormous simplification that reduces the size of the parameter space needed to summarize the data. Thus, even though it is not likely that the shear in full-field V1 and V2 is strictly azimuthal, this simple *ansatz* has allowed us to obtain a statistically reliable summary of the F99UA1 data set, and has also worked well in preliminary analysis of human parafoveal fMRI data in V1, V2, and V3 (Polimeni et al., 2005).

4.2.3. Fully general shear function

In V1, it is unlikely that the shear is uniform as is assumed in the basic uniform-shear Wedge–Dipole model. For example, it may be that the monocular crescent, lacking two independent monocular afferent inputs, has a fundamentally different pattern of shear than the parafoveal representation. If so, then the closed-form analytic expressions developed in this report will need to be improved by a more general numerical solution.

To generalize the numerical methods outlined above, we can exploit our ability to decompose quasiconformal maps into an independent conformal component and shear component and model each independently. Since we assume that the underlying shear distribution is orderly and changes slowly across cortex, then the remaining task is to find a simple model for the shear component, using as few parameters as possible. However, if the shear map was fully free to vary in a point-to-point manner, then any fitting function—e.g., a two-dimensional polynomial, a triangular mesh (Van Essen et al., 1984), or an affine image warp (Adams & Horton, 2003b)—with enough degrees of freedom, would suffice to characterize the shear, and there would be no great utility in using a conformal-plus-shear decomposition. Simple, closed-form models, such as the one presented in this report, serve as a useful conceptual guide, since full numerical solutions, while more accurate, provide much less insight or understanding.

4.3. Dipole structures in visual areas

4.3.1. Mapping singularities

One insight provided by the visuotopic mapping of the Wedge–Dipole model is that it leads us to a possible functional relationship between mapping singularities and topographic shear. The points $z = -a$ and $z = -b$ in the wedge representation's coordinate system locate *logarithmic singularities* of the dipole mapping—at these points the dipole mapping takes on an infinite value, i.e., $\log(0) = -\infty$ and $\log(1/0) = +\infty$. One interpretation of the role of the wedge mapping is that it acts to alter the domain of the map function by splitting the contralateral visual hemi-field representation in V2 along the horizontal meridian and shearing it away from the singularities.

In Fig. 19, we show that reduction of the compressive azimuthal shear causes the V2 wedge to expand toward the dipole mapping singularities located along the negative real axis. This causes the surface area of the V2 cortical representation to markedly expand. Note that the area of the cortical representation increases non-linearly with the azimuthal shear parameter α_2.

Finally, when the azimuthal shear is reduced to the point where the V2 wedge mapping is conformal, the V2 wedge encroaches upon the singularities, causing the area of V2 under the dipole mapping to approach infinity. In this case, the a-parameter singularity, lying near the foveal representation, is mapped to $\log(0) = -\infty$, whereas the b-parameter singularity in the peripheral representation is mapped to $\log(1/0) = +\infty$. This example shows that if both V1 and V2 conformally map the contralateral visual hemi-field with the dipole mapping, the presence of mapping singularities *in the mapping domain* cause the area of V2 to become infinite, thus some form of shear is necessary to deform the complex away from the singularities to prevent the map from diverging. In fact, even when the V1 mapping is approximately conformal the V2 mapping requires a significant amount of shear to compress V2 into a realistic size and shape.

Mapping singularities of this kind are not unique to the dipole mapping. In fact, most proposed models of central-

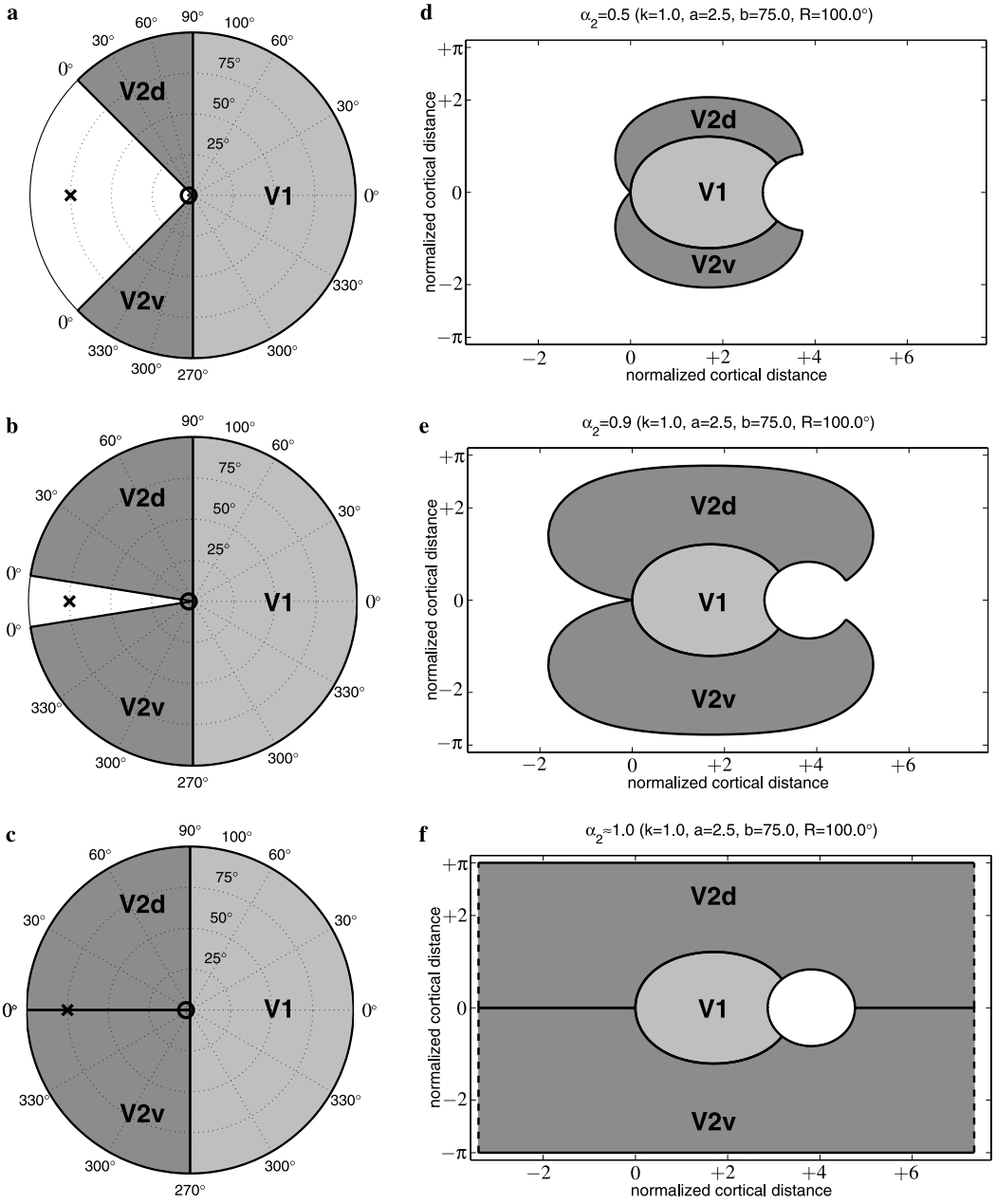

Fig. 19. Demonstration of the effect of logarithmic singularities on V2 surface area under Wedge–Dipole mapping as a function of the azimuthal shear parameter, α_2. Each row depicts a pair of wedge and dipole complexes corresponding to a given value of α_2. (A–C) The wedge complex representation of the right hemi-field of V1 and V2. Visual field coordinates representing eccentricity and azimuth appear as labeled iso-contours, with the foveal representation at the origin. The location of the logarithmic singularities corresponding to the a and b dipole parameters is denoted with the symbols "○" and "×," respectively. (D–F) The cortical representation of the two visual areas under the wedge and dipole mappings. In each dipole mapping depicted above, the mapping parameters were $k = 1$ mm/°, $a = 2.5°$, and $b = 75°$, with a maximum eccentricity of 100 ° and zero azimuthal shear in V1, $\alpha_1 = 0$ (see Mathematical Appendix for explanation of mapping parameters). (D) A moderate amount of azimuthal shear in V2 ($\alpha_2 = 0.5$) causes the area of V2 under the dipole to be comparable to that of V1, as is observed in the existing macaque data. (E) Applying less azimuthal shear ($\alpha_2 = 0.9$) results in the borders of the wedge representation closing in on the singularities, leading to a dramatic expansion of area in V2. (F) Finally, when the shear is reduced enough to allow the wedge representation of V2 to approach the singularities ($\alpha_2 = 1$), the area of the V2 cortical representation becomes infinite (see Section 4.3.1). The dashed lines represent the V2 boundary segment at infinity. This is the case in which both V1 and V2 are simultaneously conformal.

field V1 cortical magnification to date have been of the form $M(r) = k(r + a)^{-\gamma}$ along the horizontal meridian, where r represents visual eccentricity, a is a real-valued constant representing a shift in the visual field eccentricity, and the exponent γ is unity for monopole models and is near unity for other models [e.g., Van Essen et al. (1984) reported $\gamma = 1.11$]. Any isotropic two-dimensional mapping based on a linear magnification function of this form will impose a mapping singularity within the domain of the mapping of the contralateral visual hemi-field within V2.

The reported location of the singularity typically falls somewhere along the negative real axis: when $a = 0.05°$ to 4.0° (Levi et al., 1985; Schwartz, 1994; Wilson et al., 1990) the singularity is placed in the domain of the V2 mapping but outside of the domain of the V1 mapping, and when $a = 0°$ (Brewer, Press, Logothetis, & Wandell, 2002) the singularity is placed at the origin—that is, in the foveal confluence—resulting in an infinite topographic mapping for V1 as well. In either case, the mapping singularity is located in the domain of the V2 visuotopic mapping if the V2 mapping is conformal.

These models serve to characterize the topography in V1, and we have demonstrated in the present report that these mappings may be extended to characterize V2 topography as well. However, the above argument hinges upon the assumption that the V2 topographic mapping must be of the same form as the V1 mapping, which only then makes it susceptible to the divergence caused by the singularities. Why must the conformal mapping of the mirror-reversed contralateral visual hemi-field representation in V2 be identical to that of the corresponding contralateral visual hemi-field representation in V1? Is there some *other* conformal mapping for V2 topography whose singularities, if any exist, are safely outside of the mapping domain? Strikingly, the answer is negative. Because the topographic maps in V1 and V2 are identical along their shared border along the vertical meridian representation, if the V2 mapping was conformal the entire mapping of the visual hemi-field would be determined by its values along this border [by the uniqueness property of conformal mappings guaranteed by the Riemann Mapping Theorem (Ahlfors, 1966a)]. That is to say, if the V1 mapping were the dipole mapping and if the V2 mapping were conformal, the V2 mapping would also be the dipole mapping of the corresponding V2 wedge. This is why conformality is such a strong property!

In other words, if (i) the linear cortical magnification factor of the two-dimensional topographic maps in V1 and V2 is of the form $M(r) = k(r + a)^{-\gamma}$ along the horizontal meridian as explained above, (ii) the two maps are identical along the shared V1–V2 boundaries, and (iii) each map projects the contralateral visual hemi-field into cortex, then both maps cannot be locally isotropic.

The conclusion is that it is not possible for the topographic mappings of V1 and V2 to be simultaneously conformal while maintaining the observed boundary conditions and surface areas. Furthermore, if the V1 mapping is roughly conformal, the V2 mapping must be significantly sheared to achieve a representation whose surface area matches the observed surface area of V2. These observations impact areas beyond V2, such as V3, that are included in the topographic complex. The V3 mapping must exhibit substantial shear to be included in the complex without diverging, suggesting that to avoid the mapping singularities these complexes consist of a limited number of independent visual areas.

4.3.2. Topographic complexes are limited in the number of independent visual areas

The demonstration given in Fig. 19 suggests that there is a relation between the number of areas in a given topographic map complex and the amount of azimuthal shear within the individual regions. Only one member of a map complex of this form can be conformal, with shear required in the other mappings. Conversely, if multiple cortical regions were assigned a fixed amount of azimuthal shear, then the maximum number of allowable regions that can be combined into a single complex is fixed. For example, if each region exhibited a constant shear ratio of 3:1, then the number of areas that could participate in a single complex would have to be less than six to guarantee that the wedge complex would not intersect the singularities. This is because the multiple wedges must "fit" around the unit circle without "touching" the negative real axis, where the singularities associated with the parameters a and b live (see Fig. 19).

A consequence of this "scarcity" of conformality is that there is a limit to the number of visual areas that can participate in a single map complex, e.g., the V1–V2–V3 complex. This would imply that additional independent map complexes would need to exist to accommodate the large number of feature maps that exist in extra-striate cortex.

In fact, other visual areas also appear to have the structure of a dipole complex. In the owl monkey, visual areas MT and DL bear a superficial resemblance to a V1–V2 complex (see Fig. 9), as originally pointed out by Allman and Kaas (1975). However, recent studies have shown that DL may be composed of multiple cortical areas (Kaas & Morel, 1993; Sereno et al., 1994), one of which consists of a crescent-shaped subregion—known as *MTc* or *DLa*—surrounding most of MT. This area both contains a complete or nearly complete representation of the contralateral visual hemi-field and exhibits a mirror-reversed (relative to MT) topographic map across the shared border representation of the vertical meridian. This new data suggest that the area surrounding MT may be much narrower than it was originally described, implying that MTc/DLa may exhibit a larger amount of topographic shear, and that the presumptive MT–DL complex may include a greater number of visual areas.

4.3.3. Development and the dipole map function?

Why might dipole structures be a basic "design principle" in the primate visual system? The answer to this question may come from establishing a connection between flows along chemical and morphogenetic gradients, which are thought to play a critical role in neural development, and the observation that the dipole map is the steady-state solution to a diffusion equation with a single source and sink (Morse & Feshbach, 1953). More generally, the steady-state solution to the diffusion equation is a harmonic function, which, by *Dirichlet's Principle* (Courant, 1950), is the "smoothest" function satisfying the boundary conditions. A pair of harmonic

functions with complementary boundary conditions specifies a two-dimensional conformal mapping (Ahlfors, 1966a). It is for this reason that conformal topographic maps, such as the dipole map, could easily arise naturally during neural development. The anisotropy imposed by the existence of topographic shear requires only a slight extension to a non-linear diffusion equation with a spatially variable diffusion constant. Partial differential equations, such as the diffusion equation with appropriate boundary conditions, have been proposed previously as models of receptotopic map layout and formation during development [i.e., the idea of "systems matching" explored by Schwartz (1977a)].

4.4. Relationship of columnar systems and visuotopic maps

Clearly, the axes of topographic shear and the direction of columnar systems in V1 and V2 are related. But which is the prior cause?

It is widely assumed that the existence of observable topographic shear in V1 and V2, and the existence of columnar systems whose boundaries follow the principle axes of shear, are causally related, i.e., the columnar systems drive the shear. In fact, we have shown that observable shear, for example in V2, is not necessarily causally related to the existence of columnar systems in V2, as has been suggested by Roe and Ts'o (1995, 1997). The reason is that the same general form of shear would necessarily exist in any case, simply due to the shared boundary conditions and overall surface area at the level of *canonical topography* in V1 and V2 (cf. Fig. 19). Additionally, Adams and Horton (2003a) demonstrated that, in squirrel monkey, V1 retains the same shape regardless of whether or not an individual exhibits ocular dominance column stripes. It may well be that the stripe boundaries simply follow the principle axes of the topographic shear—perhaps the shear drives the layout of columnar systems, and not the other way around.

V1 shear peaks near the V1–V2 border in macaque. This may be caused by the fact that V2 shear is, on average, larger than that in V1. According to Roe and Ts'o (1995), it is several times larger; according to Shipp and Zeki (2002) and our results, the observed V2 shear is similar to the peak V1 shear (located along the V1–V2 border) observed by Blasdel and Campbell (2001) in macaque. [Blasdel and Campbell (2001) also observe that the V1 visuotopic map in squirrel monkey is nearly isotropic; however, Adams and Horton (2003b) report significant retinotopic anisotropy near the V1–V2 border of squirrel monkey visual cortex.] It may be that there is a tendency to avoid jumps in shear in the V1–V2–V3 complex, causing larger shear in V2 to "spill over" into the V1 representation across the vertical meridian. From a developmental standpoint, this would arise if the spatially variable diffusion constant governing the topographic anisotropy, as discussed above, gradually varied over the topographic complex. This hypothesis is consistent with our suggestion that the entire V1–V2–V3 complex is, from a topographic point of view, a single entity.

4.5. On publicly available data and code

The existence of publicly available data was crucial to the development of this work. The Van Essen laboratory, by providing a unique public data resource (see Van Essen, 2002), have taken an important step in the direction of "reproducible research" (Schwab, Karrenbach, & Claerbout, 2000) by providing public data sets on their web site.

We make a small step in this direction by providing the code for the Wedge–Dipole model in the Mathematical Appendix, and we are in the process of providing the remaining components of our computational environment (e.g., our near-isometric brain flattening software) on our laboratory's web site, http://eslab.bu.edu. We feel that it is increasingly important, in computational neuroscience, to provide publicly available code, since the vast majority of modeling studies currently do not do so, thereby making it difficult to verify computational claims.

4.6. Comparison of macaque and human topography

Contemporary fMRI studies have demonstrated that the two-dimensional complex logarithm models—which were originally developed to characterize macaque visuotopy—generalize to human visuotopy. Duncan and Boynton (2003) demonstrated that the monopole model provides a good fit to central-field human V1 visuotopy, but commented that a more general model extending into V2 and V3 topography was needed. Recently, Polimeni et al. (2005) jointly characterized the central-field visuotopy in human V1, V2, and V3, estimating the value of a for human visual cortex to be $0.62° \pm 0.15°$ over eight hemispheres. Interestingly, Duncan and Boynton (2003) independently estimated a for human V1 to be 0.76°, and the estimates of Horton and Hoyt (1991b) based on lesion studies of human V1 also present $a = 0.7°$. These values of a are very similar to the macaque values obtained in the present report for both 2DG ($a = 0.72°$) and electrophysiological data ($a = 0.75°$), indicating a convergence in the estimates of cortical magnification factor whereas previous estimates have been widely scattered in the range of $a = 0.05°$ to 4.0° (Gulyàs, 1997; Levi et al., 1985; Schwartz, 1994; Wilson et al., 1990).

The cortical magnification factor of the visuotopic map, defined by Daniel and Whitteridge (1961) as the ratio of the difference in cortical position to visual field position of a small movement of a visual stimulus, is itself dependent upon the size of whichever retinotopic area it describes. If, for example, two subjects have identical retinotopic mappings that differ only by a fixed scale factor, the cortical magnification factors for each

subject will reflect this scale difference. A more effective parametric characterization of the topographic map is one that is not dependent on the overall size of the retinotopic area. The parameter a of the monopole and dipole models characterizes the *space variance* of the visuotopic mapping, in a manner similar to the E_2 parameter used in psychophysical for acuity threshold measurements (Beard, Levi, & Klein, 1997; Levi, Klein, & Aitsebaomo, 1984; Levi et al., 1985; Whitaker, Rovamo, MacVeigh, & Makela, 1992). The parameter a quantifies the percentage of V1 devoted to representing the central visual field and therefore provides a meaningful, quantitative measurement of the mapping that does not depend on the absolute size of V1. Similar remarks hold for b and the peripheral representation—the fovea and periphery are each characterized by a logarithmic singularity in this model, but with opposite sign. These observations are useful for cross-subject comparison, since significant variations in the overall surface area of V1 have been observed in macaque (e.g., Sincich, Adams, & Horton, 2003; Van Essen et al., 1984) and in human (e.g., Amunts, Malikovic, Mohlberg, Schormann, & Zilles, 2000; Stensaas, Eddington, & Dobelle, 1974). However, as noted by Horton and Hoyt (1991b), the "normalized" cortical parameter a enables meaningful, quantitative comparisons of central-field V1 visual topography across species. The currently available data indicate that, in both macaque and human, the Wedge–Dipole model extends our ability to make these comparisons by including both peripheral-field topography characterized by b and the anisotropy characterized by azimuthal shear parameters for V1, V2, and V3.

Historically, indirect estimates of "cortical magnification" within human V1 have been made through the anatomical measurement of retinal ganglion cell density (Drasdo, 1977; Rolls & Cowey, 1970; Wässle, Grünert, Röhrenbeck, & Boycott, 1990; see also Adams & Horton, 2003b; Azzopardi & Cowey, 1993; Perry & Cowey, 1985; Tolhurst & Ling, 1988) and through the psychophysical measurement of visual acuity, hyperacuity, and stimulus contrast sensitivity (Rovamo & Virsu, 1979; Virsu & Rovamo, 1979; Wilson et al., 1990). Most studies, however, hypothesize that these measurements correlate with one-dimensional cortical magnification factor in V1, and assume a functional form for the scalar magnification based on fits to macaque physiological data. The Wedge–Dipole model provides the more general ability to test the correlation of retinal anatomy and visual psychophysics with the two-dimensional structure of the topographic mapping throughout the full visual field representation in V1, V2, and possibly V3. Perhaps more significantly, the Wedge–Dipole model—by establishing an independent topographic shear parameter for V1, V2, and V3—introduces a tool for psychophysically discriminating which aspects of cortical visual processing are more likely to occur in a specific visual area by measuring the dependence of behavioral performance on the anisotropy of the visual stimulus, since the a and b parameters are common to V1, V2 and V3.

One of the goals of the present work is to achieve an accurate functional form for topographic maps with a small number of parameters for use in high-precision fMRI studies of cortical visuotopy. Minimizing the parameter count is crucial to statistical fitting, given the relatively sparse and often noisy data available from both electrophysiology and fMRI. High field strength (7T) fMRI measurements of human V1 have already been demonstrated (Polimeni et al., 2005), and it is certain that in the near future much more detailed and accurate data will be available, underscoring the need for a careful parametric treatment that respects the two-dimensional structure of cortical topography.

Acknowledgments

We thank Daniel Adams, Chris Pack, Aaron Seitz, and the anonymous reviewers for their many insightful comments on this manuscript. We are grateful to David Van Essen and colleagues for constructing publicly available surface-based atlases and V1–V2 visuotopic data, downloadable from http://brainmap.wustl.edu, that were used in this study. This work was supported by NIH/NIBIB Grant R01 EB001550.

Appendix A. Mathematical appendix

A.1. Wedge–Dipole model equations

The mathematical formulae describing the Wedge–Dipole mapping have been presented elsewhere (Balasubramanian et al., 2002), and are reproduced here for convenience. A purely geometrical description of the Wedge–Dipole mapping can be found in Section 2.

Any point in the right visual hemi-field can be represented by the complex variable $z = re^{i\theta} \in \mathbb{C}^1$ with $\mathrm{Re}\{z\} \geqslant 0$, where $0 \leqslant r \leqslant r_{\max}$ represents eccentricity and $-\frac{\pi}{2} \leqslant \theta \leqslant +\frac{\pi}{2}$ represents azimuth. The *wedge map* for cortical area Vn, $n = 1,2,3$, within the left cerebral hemisphere is the map $\Lambda_n : \mathbb{C}^1 \to \mathbb{C}^1$ given by

$$\Lambda_n(re^{i\theta}) = re^{i\Theta_n(\theta)}, \tag{3}$$

where the angle function Θ_1 for V1 is given by

$$\Theta_1(\theta) = \alpha_1\theta, \tag{4}$$

the function Θ_2 for V2 is given by

$$\Theta_2(\theta) = \begin{cases} -\alpha_2^{\mathrm{V}}(\theta - \frac{\pi}{2}) + \Theta_1(+\frac{\pi}{2}) & \text{if } 0^+ \leqslant \theta \leqslant +\frac{\pi}{2}, \\ -\alpha_2^{\mathrm{D}}(\theta + \frac{\pi}{2}) + \Theta_1(-\frac{\pi}{2}) & \text{if } -\frac{\pi}{2} \leqslant \theta \leqslant 0^-, \end{cases} \tag{5}$$

and the function Θ_3 for V3 is given by

$$\Theta_3(\theta) = \begin{cases} \alpha_3^{\mathrm{V}}\theta + \Theta_2(0^+) & \text{if } 0^+ \leqslant \theta \leqslant +\frac{\pi}{2}, \\ \alpha_3^{\mathrm{D}}\theta + \Theta_2(0^-) & \text{if } -\frac{\pi}{2} \leqslant \theta \leqslant 0^-, \end{cases} \tag{6}$$

where $0^+ \equiv \lim 0 + |\varepsilon|$ and $0^- \equiv \lim 0 - |\varepsilon|$ as $\varepsilon \to 0$. As described in Section 3, the shear parameters α_n^{V} and α_n^{D} control the amount of uniform azimuthal shear within the ventral and dorsal sections of Vn. Here, we assume that the shear in the ventral and dorsal quadrants of V1 is symmetric, i.e., $\alpha_1^{\mathrm{V}} = \alpha_1^{\mathrm{D}} = \alpha_1$. Note that for any given region, $\alpha < 1$ corresponds to a compression and $\alpha > 1$ corresponds to an expansion. Here, we consider only compressive azimuthal shearing, but expansive shearing is possible within this framework.

For a point in the visual hemi-field represented by the complex coordinate z_0, the wedge map $\xi_1 = \Lambda_1(z_0)$, where $\xi_1 \in \mathbb{C}^1$, provides the complex coordinate of the corresponding point within the V1 wedge, and similarly the mapping functions $\xi_2 = \Lambda_2(z_0)$ and $\xi_3 = \Lambda_3(z_0)$, where $\xi_2, \xi_3 \in \mathbb{C}^1$, provide the coordinate transformations of the point into V2 and V3, respectively. The wedge coordinates are subsequently fed into the standard dipole mapping $\mathrm{DPL} : \mathbb{C}^1 \to \mathbb{C}^1$, which is a function $\mathrm{DPL} = \mathrm{DPL}(\xi,a,b)$ of one complex-valued variable $\xi \in \mathbb{C}^1$, and two real parameters $a, b \in \mathbb{R}^1$, given by

$$w_n = \mathrm{DPL}(\xi_n, a, b) = \log\left(\frac{\xi_n + a}{\xi_n + b}\right), \tag{7}$$

where $w_n \in \mathbb{C}^1$ signifies the complex coordinate for the nth visual area Vn in the contralateral visual cortex. The two real parameters of the dipole mapping, a and b, are *global* parameters for the topographic complex that apply to all cortical areas V1 through Vn. (The cortical mapping for the opposite visual hemi-field and corresponding cortical hemisphere is easily constructed by substituting $z \mapsto -\bar{z}$ and $w_n \mapsto -\overline{w_n}$.)

In addition to the mapping parameters, in practice the Wedge–Dipole model may also include four position parameters for the global scale ($k \in \mathbb{R}^+$), rotation ($\varphi \in [0, 2\pi) \subset \mathbb{R}^1$), and translation ($\tau \in \mathbb{C}^1$) of the dipole coordinates with respect to the cortical surface. These parameters do not affect the shape of the topographic complex or the relative surface areas between cortical regions, but rather are used to fix the absolute distances (typically in units of mm) for the model. When computing the optimal parameters to fit the Wedge–Dipole model to existing data, these global positional parameters are employed, as discussed in Section 3.

A.2. Unpinching map equations

This section summarizes the mathematical details of the unpinching map presented in Section 4. The goal of the unpinching map is to expand V2 within the dipole complex at the foveal representation such that it wraps around V1 roughly evenly along the entire extent of their shared border, thus eliminating the "pinch" exhibited at the fovea of V2 that can been seen in Fig. 5. This is accomplished by manipulating the wedge complex prior to the application of the dipole mapping.

If $\xi_1 \in \mathscr{W}_1 \subset \mathbb{C}^1$ is the complex coordinate of the V1 wedge and $\xi_2 \in \mathscr{W}_2 \subset \mathbb{C}^1$ is the complex coordinate of the V2 wedge, then under the eccentric power function,

$$\xi_1' = (\xi_1 + \delta)^\beta \tag{8.a}$$

for V1, and for V2,

$$\xi_2' = (\xi_2 + \delta)^\beta \tag{8.b}$$

such that $\xi_1', \xi_2' \in \mathbb{C}^1$ denote the complex coordinates for the V1 and V2 representations of the unpinched wedge complex, and the parameters $\beta, \delta \in \mathbb{R}^+$ control the unpinching. The output of the unpinching map may then be fed into the dipole mapping function described above.

Appendix B. Example code for Wedge–Dipole mapping

As an example of how to compute the Wedge–Dipole mapping of visual field coordinates to cortical coordinates, we have included the following code listing for MATLAB (The MathWorks, Natick, MA) (Fig. 20). The

```
%%% set default parameters
k = 15.0;      % global map scale parameter "k"

a =  0.5;      % global map parameter "a"
b = 80.0;      % global map parameter "b"

alpha1 = 1.000;   % azimuthal shear in V1
alpha2 = 0.333;   % azimuthal shear in V2
alpha3 = 0.250;   % azimuthal shear in V3

ecc  = 90;   % extent of visual field eccentricity
Necc = 20;   % number of steps in eccentricity
Npol = 22;   % number of steps in polar angle

%%% compute derived shear parameters
phi1 = (pi/2) * ( 1 - alpha1 );
phi2 = (pi/2) * ( 1 - alpha2 );
phi3 = (pi/2) * ( 1 - alpha3 );

%%% build real "r" and "theta" coordinate vectors
% create "r" exponentially spaced in [0, "ecc"]
radius = linspace(log(a), log(ecc+a), Necc)';
r = ( exp(radius) - a );

% create "theta" linearly spaced in [-pi/2, +pi/2]
theta = [linspace(-pi/2, -eps*1e5, Npol/2), ...
         linspace(+eps*1e5, +pi/2, Npol/2)];

% build vectors of polar angles relabeled by shearing
thetaV1 = (alpha1*theta);
thetaV2 = (alpha2*theta) + ...
          (sign(theta)*( phi2+phi1 ));
thetaV3 = (alpha3*theta) + ...
          (sign(theta)*( pi-phi1-phi2 ));

%%% compute complex coordinates and mappings
% visual field
z = r*exp(i*theta);

% wedge mapping
zV1 =        r*exp(i*thetaV1);
zV2 = -conj( r*exp(i*thetaV2) );
zV3 =        r*exp(i*thetaV3);

% dipole mapping
wV1 = k*log( (zV1+a)./(zV1+b) ) - k*log(a/b);
wV2 = k*log( (zV2+a)./(zV2+b) ) - k*log(a/b);
wV3 = k*log( (zV3+a)./(zV3+b) ) - k*log(a/b);
```

Fig. 20. Example MATLAB code for Wedge–Dipole mapping.

mapping itself requires three global parameters, `k`, `a`, and `b`, and three shear parameters, `alpha1`, `alpha2`, and `alpha3`, as discussed in the previous section of the Appendix, as well as three additional discretization parameters, `ecc`, `Necc`, and `Npol`. The output is an array containing the visual field coordinates, `z`, three arrays containing the wedge representations, `zV1`, `zV2`, and `zV3`, and three arrays containing the cortical representations, `wV1`, `wV2`, and `wV3`.

References

Adams, D. L. & Horton, J. C. (2001). "What you see . . .", review of *Visual Disturbances following Gunshot Wounds of the Cortical Visual Area* by Tatsuji Inouye (M. Glickstein, & M. Fahle, Trans). *Nature, 412*(6846), 482–483.

Adams, D. L., & Horton, J. C. (2002). Shadows cast by retinal blood vessels mapped in primary visual cortex. *Science, 298*(5593), 572–576.

Adams, D. L., & Horton, J. C. (2003a). Capricious expression of cortical columns in the primate brain. *Nature Neuroscience, 6*(2), 113–114.

Adams, D. L., & Horton, J. C. (2003b). A precise retinotopic map of primate striate cortex generated from the representation of angioscotomas. *Journal of Neuroscience, 23*(9), 3771–3789.

Ahlfors, L. V. (1966a). *Complex analysis* (2nd ed.). New York: McGraw-Hill.

Ahlfors, L. V. (1966b). *Lectures on quasiconformal mappings*. Princeton, N.J: Van Nostrand.

Ahlfors, L. V., & Bers, L. (1960). Riemann's mapping theorem for variable metrics. *Annals of Mathematics, 72*(2), 385–404.

Allman, J. M., & Kaas, J. H. (1974a). The organization of the second visual area (V II) in the owl monkey: a second order transformation of the visual hemifield. *Brain Research, 76*(2), 247–265.

Allman, J. M., & Kaas, J. H. (1974b). A crescent-shaped cortical visual area surrounding the middle temporal area (MT) in the owl monkey (*Aotus trivirgatus*). *Brain Research, 81*(2), 199–213.

Allman, J. M., & Kaas, J. H. (1975). The dorsomedial cortical visual area: a third tier area in the occipital pole of the owl monkeys (*Aotus trivirgatus*). *Brain Research, 100*(3), 473–487.

Amunts, K., Malikovic, A., Mohlberg, H., Schormann, T., & Zilles, K. (2000). Brodmann's areas 17 and 18 brought into stereotaxic space–where and how variable? *NeuroImage, 11*(1), 66–84.

Azzopardi, P., & Cowey, A. (1993). Preferential representation of the fovea in the primary visual cortex. *Nature, 361*(6414), 719–721.

Balasubramanian, M., Polimeni, J. R., & Schwartz, E. L. (2002). The V1–V2–V3 complex: quasiconformal dipole maps in primate striate and extra-striate cortex. *Neural Networks, 15*(10), 1157–1163.

Balasubramanian, M., Polimeni, J. R., & Schwartz, E. L. (2005). Efficient quasi-isometric flattening of large-scale cortical surfaces [Abstract]. *NeuroImage, 26*(1), S751.

Beard, B. L., Levi, D. M., & Klein, S. A. (1997). Vernier acuity with non-simultaneous targets: the cortical magnification factor estimated by psychophysics. *Vision Research, 37*(3), 325–346.

Blasdel, G., & Campbell, D. (2001). Functional retinotopy of monkey visual cortex. *Journal of Neuroscience, 21*(20), 8286–8301.

Brewer, A. A., Press, W. A., Logothetis, N. K., & Wandell, B. A. (2002). Visual areas in macaque cortex measured using functional magnetic resonance imaging. *Journal of Neuroscience, 22*(23), 10416–10426.

Courant, R. (1950). *Dirichlet's principle, conformal mapping, and minimal surfaces*. New York: Interscience Publishers.

Daniel, M., & Whitteridge, D. (1961). The representation of the visual field on the cerebral cortex in monkeys. *Journal of Physiology, 159*, 203–221.

Dow, B., Vautin, R. G., & Bauer, R. (1985). The mapping of visual space onto foveal striate cortex in the macaque monkey. *Journal of Neuroscience, 5*(4), 890–902.

Drasdo, N. (1977). The neural representation of visual space. *Nature, 266*(5602), 554–556.

Drasdo, N., & Fowler, C. W. (1974). Non-linear projection of the retinal image in a wide-angle schematic eye. *British Journal of Ophthalmology, 58*(8), 709–714.

Duncan, R. O., & Boynton, G. M. (2003). Cortical magnification within human primary visual cortex correlates with acuity thresholds. *Neuron, 38*(4), 659–671.

Engel, S. A., Glover, G. H., & Wandell, B. A. (1997). Retinotopic organization in human visual cortex and the spatial precision of functional MRI. *Cerebral Cortex, 7*(2), 181–192.

Engel, S. A., Rumelhart, D. E., Wandell, B. A., Lee, A. T., Glover, G. H., Chichilnisky, E. J., et al. (1994). fMRI of human visual cortex. *Nature, 369*(6481), 525.

Fox, P. T., Miezin, F. M., Allman, J. M., Van Essen, D. C., & Raichle, M. E. (1987). Retinotopic organization of human visual cortex mapped with positron emission tomography. *Journal of Neuroscience, 7*(3), 913–922.

Gattass, R., Gross, C. G., & Sandell, J. H. (1981). Visual topography of V2 in the macaque. *Journal of Comparative Neurology, 201*(4), 519–539.

Gattass, R., Sousa, A. P., & Gross, C. G. (1988). Visuotopic organization and extent of V3 and V4 of the macaque. *Journal of Neuroscience, 8*(6), 1831–1845.

Glickstein, M., & Whitteridge, D. (1987). Tatsuji Inouye and the mapping of the visual field on the human cerebral cortex. *Trends in Neurosciences, 10*(9), 350–353.

Gulyàs, B. (1997). Functional organization of human visual cortical areas. In: K. S. Rockland, J. H. Kaas, & A. Peters (Eds.), *Extrastriate Cortex in Primates*. Vol. 12. *Cerebral Cortex* (pp. 743–775). New York: Kluwer Academic/Plenum Publishers.

Hastie, T., Tibshirani, R., & Friedman, J. H. (2001). *The Elements of statistical learning*. New York: Springer.

Holmes, G., & Lister, W. T. (1916). Disturbances of vision from cerebral lesions with special reference to the cortical representation of the macula. *Brain, 39*, 34–73.

Horton, J. C., Dagi, L. R., McCrane, E. P., & de Monasterio, F. M. (1990). Arrangement of ocular dominance columns in human visual cortex. *Archives of Ophthalmology, 108*(7), 1025–1031.

Horton, J. C., & Hocking, D. R. (1996). Intrinsic variability of ocular dominance column periodicity in normal macaque monkeys. *Journal of Neuroscience, 16*(22), 7228–7239.

Horton, J. C., & Hoyt, W. F. (1991a). Quadrantic visual field defects: a hallmark of lesions in extrastriate (V2/V3) cortex. *Brain, 114*(4), 1703–1718.

Horton, J. C., & Hoyt, W. F. (1991b). The representation of the visual field in human striate cortex. A revision of the classic Holmes map. *Archives of Ophthalmology, 109*(6), 816–824.

Howard, I. P., & Rogers, B. J. (1995). *Binocular vision and stereopsis*. New York: Oxford University Press.

Hubel, D. H., & Wiesel, T. N. (1977). Ferrier lecture: Functional architecture of macaque monkey visual cortex. *Proceedings of the Royal Society of London Series B, Biological Sciences, 198*(1130), 1–59.

Hubel, D. H., Wiesel, T. N., & LeVay, S. (1974). Visual-field representation in layer IVC of monkey striate cortex [Abstract]. *Society for Neuroscience Abstracts*.

Inouye, T. (1909). *Die Sehstörungen bei Schssverletzungen der Kortikalen Sehsphäre nach Beobachtungen an Verwundeten der Letzten Japanischen Kriege*. Leipzig: W. Engelmann. *Visual disturbances following gunshot wounds of the cortical visual area* (English translation by M. Glickstein & M. Fahle). Brain (Supplement) 123, Oxford University Press, 2000.

Kaas, J. H. (1997). Theories of visual cortex organization in primates. In: K. S. Rockland, J. H. Kaas, & A. Peters (Eds), *Extrastriate Cortex in Primates*. Vol. 12. *Cerebral Cortex* (pp. 91–125). New York: Kluwer Academic/Plenum Publishers.

Kaas, J. H., & Morel, A. (1993). Connections of visual areas of the upper temporal lobe of owl monkeys: the MT crescent and dorsal

and ventral subdivisions of FST. *Journal of Neuroscience, 13*(2), 534–546.

Kythe, P. K. (1998). *Computational conformal mapping*. Boston: Birkhäuser.

Lagarias, J. C., Reeds, J. A., Wright, M. H., & Wright, P. E. (1998). Convergence properties of the Nelder-Mead simplex method in low dimensions. *SIAM Journal of Optimization, 9*(1), 112–147.

Landau, P., & Schwartz, E. L. (1992). Computer simulation of cortical polymaps: a proto-column algorithm. *Neural Networks, 5*(2), 187–206.

Landau, P., & Schwartz, E. L. (1994). Subset warping: rubber sheeting with cuts. *CVGIP: Graphical Models and Image Processing, 56*(3), 247–266.

Letelier, J. C., & Varela, F. (1984). Why the cortical magnification factor in rhesus is isotropic. *Vision Research, 24*(9), 1091–1095.

LeVay, S., Hubel, D. H., & Wiesel, T. N. (1975). The pattern of ocular dominance columns in macaque visual cortex revealed by a reduced silver stain. *Journal of Comparative Neurology, 159*(4), 559–576.

Levi, D. M., Klein, S. A., & Aitsebaomo, A. P. (1984). Detection and discrimination of the direction of motion in central and peripheral vision of normal and amblyopic observers. *Vision Research, 24*(8), 789–800.

Levi, D. M., Klein, S. A., & Aitsebaomo, A. P. (1985). Vernier acuity, crowding and cortical magnification. *Vision Research, 25*(7), 963–977.

Mallot, H. A. (1985). An overall description of retinotopic mapping in the cat's visual cortex areas 17, 18, and 19. *Biological Cybernetics, 52*(1), 45–51.

Milnor, J. (1969). A problem in cartography. *American Mathematical Monthly, 76*(10), 1011–1112.

Morse, P. M., & Feshbach, H. (1953). *Methods of theoretical physics*. McGraw-Hill.

Nelder, J. A., & Mead, R. (1965). A simplex method for function minimization. *Computer Journal, 7*, 308–313.

Ogawa, S., Tank, D. W., Menon, R., Ellermann, J. M., Kim, S., Merkle, H., et al. (1992). Intrinsic signal changes accompanying sensory stimulation: functional brain mapping with magnetic resonance imaging. *Proceedings of the National Academy of Sciences of the United Stats of America, 89*(13), 5951–5955.

Pearson, C. E. (1982). Optimal mapping from a sphere onto a plane. *SIAM Review, 24*(4), 469–475.

Perry, V. H., & Cowey, A. (1985). The ganglion cell and cone distributions in the monkey's retina: implications for central magnification factors. *Vision Research, 25*(12), 1795–1810.

Polimeni, J. R., Balasubramanian, M., & Schwartz, E. L. (2003). Full-field two-dimensional V1, V2, and V3 visuotopy represented by a quasiconformal map complex [Abstract]. *Society for Neuroscience Abstracts*.

Polimeni, J. R., Hinds, O. P., Balasubramanian, M., van der Kouwe, A. J., Wald, L. L., Dale, A. M., Fischl, B., & Schwartz, E. L. (2005). The human V1–V2–V3 visuotopic map complex measured via fMRI at 3 and 7 Tesla [Abstract]. *Society for Neuroscience Abstracts*.

Polyak, S. L. (1941). *The retina: the anatomy and the histology of the retina in man, ape, and monkey, including the consideration of visual functions, the history of physiological optics, and the histological laboratory technique*. University of Chicago Press.

Roe, A. W., & Ts'o, D. Y. (1995). Visual topography in primate V2: multiple representations across functional stripes. *Journal of Neuroscience, 15*(5), 3689–3715.

Roe, A. W., & Ts'o, D. Y. (1997). The functional architecture of area V2 in the macaque monkey: physiology, topography, and connectivity. In: K. S. Rockland, J. H. Kaas, & A. Peters (Eds.), *Extrastriate Cortex in Primates*. Vol. 12. *Cerebral Cortex* (pp. 295–333). New York: Kluwer Academic/Plenum Publishers.

Rojer, A. S., & Schwartz, E. L. (1990). Design considerations for a space-variant visual sensor with complex-logarithmic geometry. In: *Proceedings of the 10th International Conference on Pattern Recognition* (pp. 278–285). Vol. 2.

Rolls, E. T., & Cowey, A. (1970). Topography of the retina and striate cortex and its relationship to visual acuity in rhesus monkeys and squirrel monkeys. *Experimental Brain Research, 10*(3), 298–310.

Rosa, M. (1997). Visuotopic organization of primate extrastriate cortex. In: K. S. Rockland, J. H. Kaas, & A. Peters (Eds.), *Extrastriate Cortex in Primates*. Vol. 12. *Cerebral Cortex* (pp. 127–203). New York: Kluwer Academic/Plenum Publishers.

Rosa, M. G. P., Sousa, A. P. B., & Gattass, R. (1988). Representation of the visual field in the second visual area of the *Cebus* monkey. *Journal of Comparative Neurology, 275*, 326–345.

Rovamo, J., & Virsu, V. (1979). An estimation and application of the human cortical magnification factor. *Experimental Brain Research, 37*(3), 495–510.

Sakitt, B. (1982). Why the cortical magnification factor in rhesus can not be isotropic. *Vision Research, 22*(3), 417–421.

Schreiber, K., Crawford, J. D., Fetter, M., & Tweed, D. (2001). The motor side of depth vision. *Nature, 410*(6830), 819–822.

Schwab, M., Karrenbach, N., & Claerbout, J. (2000). Making scientific computations reproducible. *Computing in Science and Engineering, 2*(6), 61–67.

Schwartz, E. L. (1977a). The development of specific visual projections in the monkey and the goldfish: outline of a geometric theory of receptotopic structure. *Journal of Theoretical Biology, 69*(4), 655–685.

Schwartz, E. L. (1977b). Spatial mapping in primate sensory projection: analytic structure and relevance to perception. *Biological Cybernetics, 25*(4), 181–194.

Schwartz, E. L. (1980). Computational anatomy and functional architecture of striate cortex: a spatial mapping approach to perceptual coding. *Vision Research, 20*(8), 645–669.

Schwartz, E. L. (1981). Positron emission tomography studies of human visual cortex [Abstract]. *Society for Neuroscience Abstracts*.

Schwartz, E. L. (1983). Cortical mapping and perceptual invariance: a reply to Cavanagh. *Vision Research, 23*(8), 831–835.

Schwartz, E. L. (1984). Anatomical and physiological correlates of visual computation from striate to infero-temporal cortex. *IEEE Transactions on Systems, Man and Cybernetics, 14*(2), 257–271.

Schwartz, E. L. (1985). On the mathematical structure of the visuotopic mapping of macaque striate cortex. *Science, 227*(4690), 1065–1066.

Schwartz, E. L. (1994). Computational studies of the spatial architecture of primate visual cortex: Columns, maps, and protomaps. In: A. Peters, & K. S. Rockland (Eds.), *Primary Visual Cortex in Primates*. Vol. 10. *Cerebral Cortex* (pp. 359–411). New York: Kluwer Academic/Plenum Publishers.

Schwartz, E. L., Christman, D. R., & Wolf, A. P. (1984). Human primary visual cortex topography imaged via positron tomography. *Brain Research, 294*(2), 225–230.

Schwartz, E. L., Munsiff, A., & Albright, T. (1989a). The topographic map of macaque V1 measured via 3D computer reconstruction of 2DG serial sections, numerical flattening of cortex, and conformal image modeling [Abstract]. *Investigative Ophthalmology and Visual Science, 30*(3), S298.

Schwartz, E. L., Shaw, A., & Wolfson, E. (1989b). A numerical solution to the generalized mapmaker's problem: flattening nonconvex polyhedral surfaces. *IEEE Transactions on Pattern Analysis and Machine Intelligence, 11*(9), 1005–1008.

Segel, L. A. (1977). *Mathematics applied to continuum mechanics*. New York: Macmillan Publishing.

Sereno, M. I., Dale, A. M., Reppas, J. B., Kwong, K. K., Belliveau, J. W., Brady, T. J., et al. (1995). Borders of multiple visual areas in humans revealed by functional magnetic resonance imaging. *Science, 268*(5212), 889–893.

Sereno, M. I., McDonald, C. T., & Allman, J. M. (1994). Analysis of retinotopic maps in extrastriate cortex. *Cerebral Cortex, 4*(6), 601–620.

Shipp, S., & Zeki, S. (2002). The functional organization of area V2, II: the impact of stripes on visual topography. *Visual Neuroscience, 19*(2), 211–231.

Sincich, L. C., Adams, D. L., & Horton, J. C. (2003). Complete flatmounting of the macaque cerebral cortex. *Visual Neuroscience, 20*(6), 663–686.

Sincich, L. C., & Horton, J. C. (2002). Pale cytochrome oxidase stripes in V2 receive the richest projection from macaque striate cortex. *Journal of Comparative Neurology, 447*(1), 18–33.

Stensaas, S. S., Eddington, D. K., & Dobelle, W. H. (1974). The topography and variability of the primary visual cortex in man. *Journal of Neurosurgery, 40*(6), 747–755.

Symm, G. T. (1966). An integral equation method in conformal mapping. *Numerische Mathematik, 9*, 250–258.

Talbot, S. A. (1942). A lateral localization in the cat's visual cortex. *Federation Proceedings, 1*, 84.

Talbot, S. A., & Marshall, W. H. (1941). Physiological studies on neural mechanisms of visual localization and discrimination. *American Journal of Opthalmology, 24*, 1255–1263.

Tolhurst, D. J., & Ling, L. (1988). Magnification factors and the organization of the human striate cortex. *Human Neurobiology, 6*(4), 247–254.

Tootell, R. B., & Hamilton, S. L. (1989). Functional anatomy of the second visual area (V2) in the macaque. *Journal of Neuroscience, 9*(8), 2620–2644.

Tootell, R. B., Silverman, M. S., Switkes, E., & DeValois, R. (1985). Rejoinder [letter in reply to Schwartz, E. L., "On the mathematical structure of the visuotopic mapping of macaque striate cortex". *Science, 227*(4690), 1065–1066]. *Science, 227*(4690), 1066.

Tootell, R. B., Silverman, M. S., Switkes, E., & DeValois, R. L. (1982). Deoxyglucose analysis of retinotopic organization in primate striate cortex. *Science, 218*(4575), 902–904.

Tootell, R. B., Switkes, E., Silverman, M. S., & Hamilton, S. L. (1988). Functional anatomy of macaque striate cortex. II. Retinotopic organization. *Journal of Neuroscience, 8*(5), 1531–1568.

Van Essen, D. C. (2002). Windows on the brain: the emerging role of atlases and databases in neuroscience. *Current Opinion in Neurobiology, 12*(5), 574–579.

Van Essen, D. C., Felleman, D. J., DeYoe, E. A., Olavarria, J., & Knierim, J. (1990). Modular and hierarchical organization of extrastriate visual cortex in the macaque monkey. *Cold Spring Harbor Symposium on Quantitative Biology, 55*, 679–696.

Van Essen, D. C., Newsome, W. T., & Maunsell, J. H. R. (1984). The visual representation in striate cortex of the macaque monkey: asymmetries, anisotropies, and individual variability. *Vision Research, 24*(5), 429–448.

Van Rijn, L. J., & Van den Berg, A. V. (1993). Binocular eye orientation during fixations: Listing's law extended to include eye vergence. *Vision Research, 33*(5-6), 691–708.

Virsu, V., & Rovamo, J. (1979). Visual resolution, contrast sensitivity, and the cortical magnification factor. *Experimental Brain Research, 37*(3), 475–494.

Wandell, B. A., Brewer, A. A., & Dougherty, R. F. (2005). Visual field map clusters in human cortex. *Philosophical transactions of the Royal Society of London Series B, Biological Sciences, 360*(1456), 693–707.

Wässle, H., Grünert, U., Röhrenbeck, J., & Boycott, B. B. (1990). Retinal ganglion cell density and cortical magnification factor in the primate. *Vision Research, 30*(11), 1897–1911.

Whitaker, D., Rovamo, J., MacVeigh, D., & Makela, P. (1992). Spatial scaling of vernier acuity tasks. *Vision Research, 32*(8), 1481–1491.

Wilson, H., Levi, D., Maffei, L., Rovamo, J., & DeValois, R. (1990). The perception of form: retina to striate cortex. In L. Spillman & J. S. Werner (Eds.), *Visual perception: The neurophysiological foundations* (pp. 231–272). New York: Academic Press.

Zeki, S. M. (1969). Representation of central visual fields in prestriate cortex of monkey. *Brain Research, 14*(2), 271–291.